ET163005 & ET163007_DSHC_(EIS analysis to find the effect of compression temp on P25 based DSSC)_Final report

by liuc Central Library

Submission date: 02-Oct-2021 07:38AM (UTC+0300)
Submission ID: 1663141884
File name: e_effect_of_compression_temp_on_P25_based_DSSC__Final_report.pdf (3.32M)
Word count: 24538
Character count: 124509

ELECTROCHEMICAL IMPEDANCE SPECTROSCOPY ANALYSIS TO FIND THE EFFECT OF COMPRESSION TEMPERATURE ON THE PERFORMANCE OF P25 BASED DYE SENSITIZED SOLAR CELL

by

MD. INZAMAM UL ALAM CHOWDHURY

MD. MOHSIN HOSSAIN

BACHELOR OF SCIENCE IN ELECTRICAL AND ELECTRONIC ENGINEERING

Department of Electrical and Electronic Engineering
INTERNATIONAL ISLAMIC UNIVERSITY CHITTAGONG

SEPTEMBER 2021

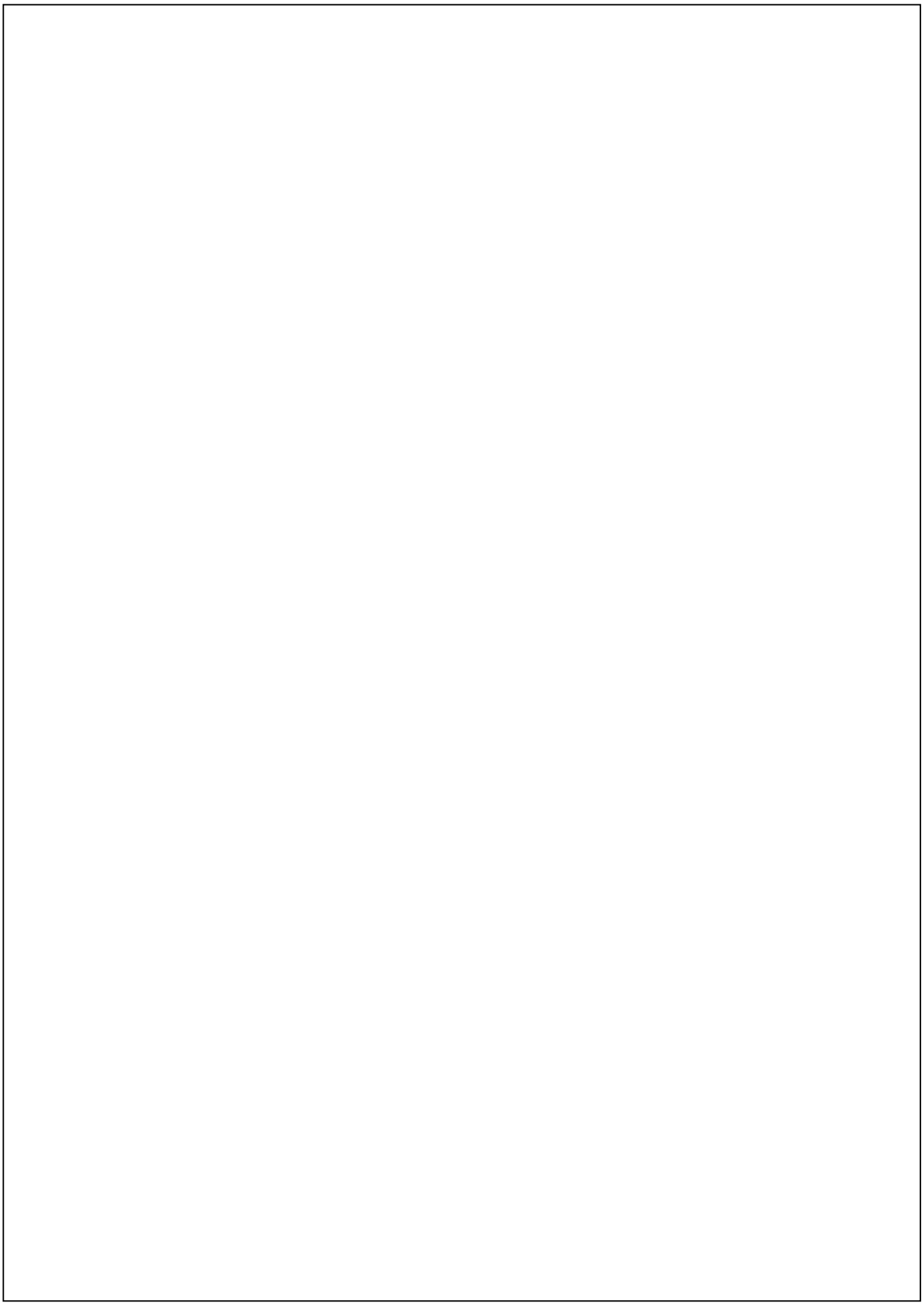

ELECTROCHEMICAL IMPEDANCE SPECTROSCOPY ANALYSIS TO FIND THE EFFECT OF COMPRESSION TEMPERATURE ON THE PERFORMANCE OF P25 BASED DYE SENSITIZED SOLAR CELL

by

MD. INZAMAM UL ALAM CHOWDHURY

MD. MOHSIN HOSSAIN

A thesis
submitted as partial fulfilment of the requirement for the degree of

BACHELOR OF SCIENCE IN ELECTRICAL AND ELECTRONIC ENGINEERING

Department of Electrical and Electronic Engineering
INTERNATIONAL ISLAMIC UNIVERSITY CHITTAGONG

SEPTEMBER 2021

CERTIFICATE OF APPROVAL

The thesis entitled as "**Electrochemical impedance spectroscopy analysis to find the effect of compression temperature on the performance of P25 based dye sensitized solar cell**" submitted by **Md. Inzamam Ul Alam Chowdhury**, bearing Matric ID. **ET 163005** and **Md. Mohsin Hossain,** bearing Matric ID. **ET 163007** of session **Autumn 2020** , to the Department of Electrical and Electronic Engineering, International Islamic University Chittagong, has been accepted as satisfactory in partial fulfilment of the requirements for the degree of Bachelor of Science in Engineering and approved for the examination held on **3rd September, 2021**.

_____

Supervisor
Dr. Md. Shamimul Haque Choudhury
Associate Professor,
Department of Electrical and Electronic Engineering
International Islamic University Chittagong

DECLARATION

It is hereby declared that this work has been done by us and no portion of the work contained in this thesis has been submitted elsewhere for the award of any degree or diploma.

_____

Md. Inzamam Ul Alam Chowdhury

_____

Md Mohsin Hossain

ACKNOWLEDGMENT

All praises and thanks to Allah, the Lord of the world, the most Beneficent, the most Merciful for helping us to accomplish this work.

We are beholden to a number of people, who supported us to carry out this work and report preparation we would like to thank our thesis supervisor Dr. Md. Shamimul Haque Choudhury, Associate Professor, Dept. of EEE, IIUC, for his enormous support and careful guidance. Without his guidance, it was almost impossible to endure the mistakes we had committed in the thesis and always encouraged us by correcting out wrong proceedings. It was only the endless support offered by him that enable us to complete this devoted task.

We are also grateful to the faculty members of the department of EEE .They were always inspirational for us.

We owe to all those authors and researchers whose work we used in designing the research and in preparing this dissertation.

We want to thank all of our family members, specially our parents for their contribution and support in completing our thesis. We thank them all in making it possible for us to carry out the research as well as enjoy such an enlightening experience.

Authors

ABSTRACT

In this investigation the effect of varying compression temperature on photovoltaic performance for TiO_2 based dye-sensitized-solar-cell (DSSC) has been observed using electrochemical impedance spectroscopy (EIS) analysis. The cells are fabricated using a new electrophoretic deposition technique that is four-layer-four-side electrophoretic deposition which ensures homogenous crack free photo electrode surface. Electrodeposited photo anodes are compressed at varying compression temperature (room temperature to 90 °C) as an post deposition treatment. From the impedance spectroscopy analysis the changes of impedance in Nyquist plot (Z′ vs. Z″) shows that due to changes in compression temperature (room temperature to 90 °C) the values of charge transfer resistance R_{ct}(AE) are reduced and that's why more electrons are conducted inside the film. Shifting of characteristics frequency peak (F_{max}) towards low frequency increases the electron life time (τ) which has been observed by increasing the compression temperature up to 70 °C. Since open circuit voltage (V_{oc}) is proportional to electron life time, with the increasing of electron life time will have higher open circuit voltage (V_{oc}) value by increasing the compression temperature up to 70 °C. The Fill Factor (FF) has been improved due to the uniformity of layers by varying the compression temperature up to 70 °C . Because of the significant improvement of open circuit voltage (V_{oc}) , photo current density (J_{sc}) and Fill Factor (FF) the overall efficiency (η) has also substantially improved by the insertion of compressed temperature up to 70 °C . The series resistance of the cell (calculated from EIS data) reduces by increasing up to 70 °C compressed heat. Similar results have been observed from the calculated series resistance from the I-V curve which is the reason for change in the photovoltaic performance. On the other hand the shunt resistance of the cell (calculated from EIS data) increases with the increasing compression temperature up to 70 °C . Thus same results have been observed from the calculated shunt resistance from the I-V curve which makes an impact for the change in the photovoltaic performance. So photovoltaic performance and parameters from impedance spectroscopy analysis and from I-V curve matches with each other. At optimum 70 °C compression temperature and 40MPa compression pressure the maximum efficiency (η) of 3.85% has been attained which gives the open circuit voltage (V_{oc}), photo current density (J_{sc}) and fill factor of 0.739 V, 9.30 mA/cm^2 and 0.58 respectively.

TABLE OF CONTENTS

LIST OF FIGURES

LIST OF TABLES

LIST OF ABBREVIATIONS

DSSC	Dye Sensitized Solar Cell
EIS	Electrochemical Impedance Spectroscopy
PCE	Power Conversion Efficiency
ITO	Indium Tin Oxide
PET	Polytheylene Terephthalate Film
SEM	Scanning Electron Microscopy
HOMO	Highest Occupied Molecule Orbital
LUMO	Lowest Unoccupied Molecule Orbital
CL	Conduction Layer
TCO	Transparent Conductive Oxide
AM	Air Mass
FTO	Flourine doped Tin Oxide
BIPV	Building Integrated Photo Voltaic Application
AS	Admittance Spectroscopy
RCE	Counter Electrode Resistance
RAE	Active Electrode Resistance
NP	Nano Particle
EPD	Electrophoretic Deposition
PCE	Power Conversion Efficiency
EQE	External Quantam Efficiency
4L4SEPD	Four Layer Four Side Electrophoretic Deposition
DOS	Density Of State
CB	Conduction Band
CDCA	Co-adsorbent additive

CHAPTER 1

INTRODUCTION

1.1 Introduction

With the increasing rate of the worldwide population, the world energy demand is growing day by day. As non-renewable energy like fossil fuel (coal, oil, gas) are running out and creating a negative impact on nature such as emitting CO_2 gas which increases global warming issues and is not sustainable, that's why renewable energy is known as conventional energy has become a focusing point for scientists because they are relying on renewable energy-based energy conservation device.

The effect of photovoltaic of solar energy harvesting was introduced by French scientist Edmond Becquerel in 1839 [1]. Three generations of solar cell are "First-generation solar cell"-Silicon (Si) based materials, "Second-generation solar cell'-semiconductor materials (CdTe, CZnTs, CIGS, GalnP, GaAs), and the third generation solar cell "Emerging materials (DSSC, Perovskite, organic)

Where by silicon (Si) base materials having high photoelectric conversion efficiency of 25%. But to get a high purity of silicon crystal structure. The first generation of solar cells appeared to be costly. A thin-film solar cell based on GaAs, CdTe, and other materials was utilized in the second generation solar cell, with an efficiency (10-20%) lower than the first generation silicon base solar cell [2],[3].

Researchers have proposed organic solar cells (11%), DSSC (13%), and perovskite sensitized cells (22%) in the third generation of solar cells, demonstrating the capacity to achieve good efficiency while reducing cost. Due to low-cost material, mechanical flexibility, ease to fabricate, etc make dye-sensitized solar cells effective regarding the improvement of efficiency and as well as photovoltaic performance too. Michel pretzel did the sensitized electrochemical PV device with TiO_2 material entitled as "Dye-sensitized solar cell" [4],[5].

The fabrication of photoanodes is done from a mesoporous structure like TiO_2, ZnO, Nb_2O_5, GaAs, Cds SnO_2[6]–[8].

TiO_2 has some good characteristics such as large catalyst band gape, and Low recombination rate, chemical strong stability, large surface area, little toxicity for DSSC [9].

Matsumura et al and Alonso et al used sintered ZnO electrodes and get less than 1% of efficiency since the dyes used at that time were unstable. Gratzel and co-workers had introduced TiO_2 electrodes with high surface area with efficiency reported(7-8%) [10].

The solar cell composed of TiO_2 having a bandgap (3.2eV) shows the most efficient material in electron-transporting in DSSC. Although a good competitor is being introduced, ZnO has almost the same injection process and band gap (3.2eV) along with TiO_2 [11]. Despite the lower density of the state, ZnO has a greater electron mobility (115-155cm2/Vs2) than TiO_2(~10~5cm^2/vs2). However, ZnO has a conversion efficiency of 0.4~5.8%, which is low compare to TiO_2. [12]–[14].

Chemical stability of TiO_2 is better than ZnO. And Dye adsorption nature of TiO_2 is much better than that of ZnO. "Recombination rate" for ZnO is much lower than that of TiO_2 .The synthesis of TiO_2 structure namely "nanoparticle" "nanorod (NRs), nanowire(NWs), nanotubes(NTS) are produced by synthetic methods like social analysis, chemical and physical vapor deposition method, etc [15].

ZnO-based DSSC efficiency was reported 5% at 1/10 sun, and 4.1% at 1 sum which tells the significant low efficiency compare to TiO_2 [16].

Several reports have been shown about the dye adsorption problem of ZnO, electron lifetime of ZnO was found higher than TiO_2 but the performance of ZnO was found less than TiO_2 base cell [16].

In the structure of DSSC, the substrate can be a glass substrate or plastic substrate but the glass substrate shows better performance comparing with the plastic substrate. The efficiency of DSSC with glass substrate is higher than that of efficiency of DSSC with plastic substrate. This is the primary cause of flexible cells' lower efficiency. As a result, a method for increasing the solar cell's efficiency introduced for DSSC sintered at (150-450)°C of TiO_2 photoelectric with ultraviolet light [17].

Later on "Hydrothermal Crystallization" for the thick film of TiO_2 crystalline base DSSC[18]. Performance improvement of DSSC based Natural dye by Clathrin protein [19], Binder fee coating of Mesoscopic Titania [20], TiO_2 /MnO_2 bilayer assembled photo anode [21], Adjusting the ratio of natural Red and Yellow dyes in a combination [22], Electrophoretic deposition of titania nanoparticle film for DSSC [23]. To increase the layer's quality including the efficiency of DSSC, Mechanical compression of TiO_2 np thin film was

introduced [24]. Later mechanical compression with annealing the compression plate, The fabrication of DSSC by hot compress method has been shown by researchers [25].

Later on, to reduce the crack issue shown in the SEM image, compression and hot compression of ZnO and TiO_2 have been done for glass substrate and plastic substrate using the electrophoretic method [26]–[28]. Later with hot compression and compression, the Electrochemical Impedance spectroscopy analysis has been shown with I-V data for ZnO [29],[30].

1.2 Objectives

The main purpose of this work is to,

Study the new electrophoretic deposition (4L4SEPD) technique and Electrochemical Impedance Spectroscopy analysis for TiO_2 base Dye-Sensitized Solar Cell, where homogenous and compact layer photo electrodes were prepared using hot compression (post-deposition) technique and also observe the I-V curve data regarding this work.

1.3 Diagram of the work:

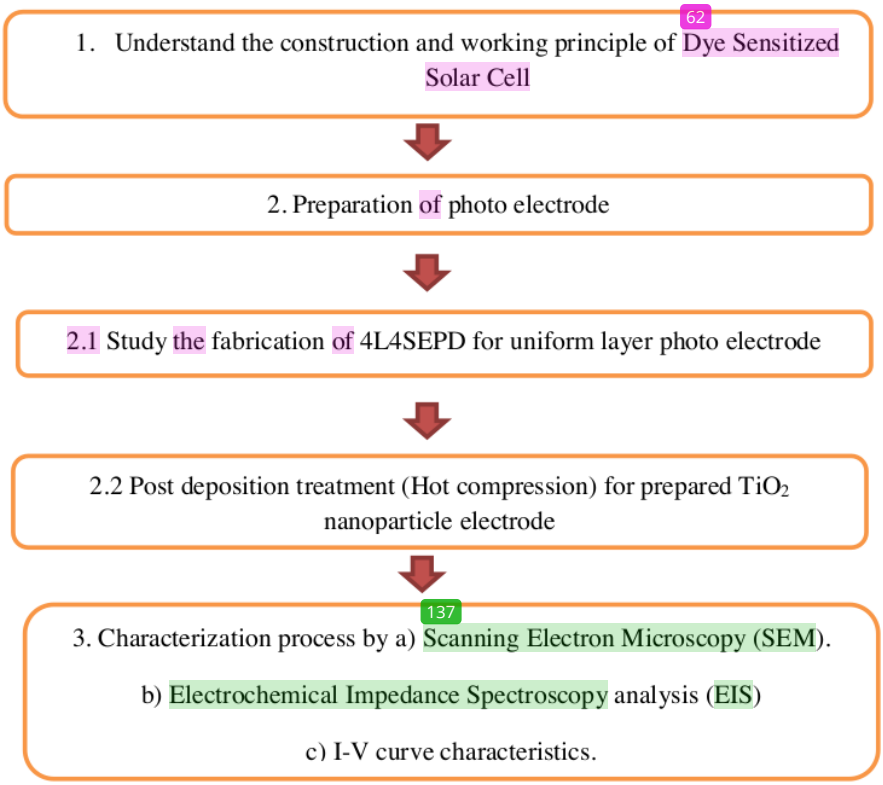

1.4. Thesis Layout

The analysis of electrochemical Impedance Spectroscopy for TiO_2 based Dye-sensitized solar cells are being distributed in five chapters. A short description of each chapter is given below

Chapter 1: "Introduction"	This introductory chapter gives an overview of the whole work including introduction, Objective, Diagram of work, thesis layout
Chapter 2: "Literature Review"	In this chapter introduction of DSSC, EPD technique, Multilayer and details overview of Electrochemical Impedance Spectroscopy(EIS) have been discussed
Chapter 3: "Experimental"	In this chapter, the full experimental methods are discussed
Chapter 4: "Result and Discussion"	In this chapter the result found from the experiment is analyzed and discussed.
Chapter 5: "Conclusion and Future work"	In this chapter comments about the whole work, the future scope of the work are discussed

CHAPTER 2

LITERATURE REVIEW

2.1 Introduction

The world has already witnessed a new generation of solar cells from the three generation of the solar cell. The third-generation solar cells are a range of novel alters natives to first-generation because despite having high efficiency the high-cost silicon p-n junction solar cell has been a major issue and second-generation solar cell (CdTe, GaAs) because they have the low-cost solution. But the efficiency of thin-film is very low. So, third-generation solar cell aims to achieve high-efficiency solar cell using materials that are non-toxic and unlimited to abundance in the earth.

Various strategies have been adopted in recent years to construct solar cells using organizing assemblies of Nano structure architecture. Which includes a cell called “Dye-sensitized solar cell”. It is the most well-known and unconventional photo voltaic system is the DSSC developed by Gratzel in 1991.

This DSSC is closely related to Nano technologies. It has demonstrated promising light-harvesting properties as the next generation of solar cells that could potentially lead to the realization of low-cost and high-efficiency properties to meet future energy demand. At the moment this unique photo electro chemical solar cell-based in TiO_2 Nano particle photo anode sensitized with a harvesting metal- organic dye is at its early commercialization stage offering an interesting alternative for existing silicon base solar cells as well as a thin-film solar cell. Despite having low conversion efficiency after doing significant experimental effort spent its performance ratio should be high enough to compete with fossil fuel electrical generation.

2.2 Solar energy and solar cell

An ever energy usage is a consequence of the world's rapidly increasing economy and population. Energy demand will soon be met by the broad deployment of renewable energy sources, according to global and regional trends. Weather and climate-driven energy sources, on the other hand, have a lot of regional and temporal variability. Hybridization of two or more energy sources into a single power station is one of the most generally discussed strategies to alleviate the mismatch between demand and supply given by renewable generating (like wind-solar, solar-hydro, or solar-wind-hydro). Renewable energy is derived

from natural processes that are replenished constantly. Renewable energy is booming, due to technological advancements that are lowering costs and delivering on the promise of a clean energy future. Renewable energy, often known as clean energy, is derived from naturally regenerated sources or processes. For example, even if their availability is dependent on time and weather, sunlight and wind continue to shine and blow.

In 1954 the first silicon photovoltaic cell was created by Bell Labs. Although solar energy had previously been absorbed and transformed into useful energy using a variety of methods, it was not until 1954 that solar power became a viable source of electricity for powering electronics for long periods. Solar cells converted solar radiation to electricity with a 4 percent efficiency; for comparison, many commonly accessible solar panels today can convert sunlight to solar power with 20% efficiency, a number that is constantly increasing.

Look at the differences between using renewable resources to generate electricity and using fossil fuels. Oil, gas, and coal took hundreds of thousands of years to develop, so each time one of these finite resources is used to generate energy, it gets a little closer to exhaustion. Using a renewable resource, such as wind, solar, or hydropower, to generate power does not deplete that resource. There will always be constant sunlight shining on the Earth's surface, and there will always be an infinite amount of sunlight to convert into electricity in the future. Given below the classification of solar cells:

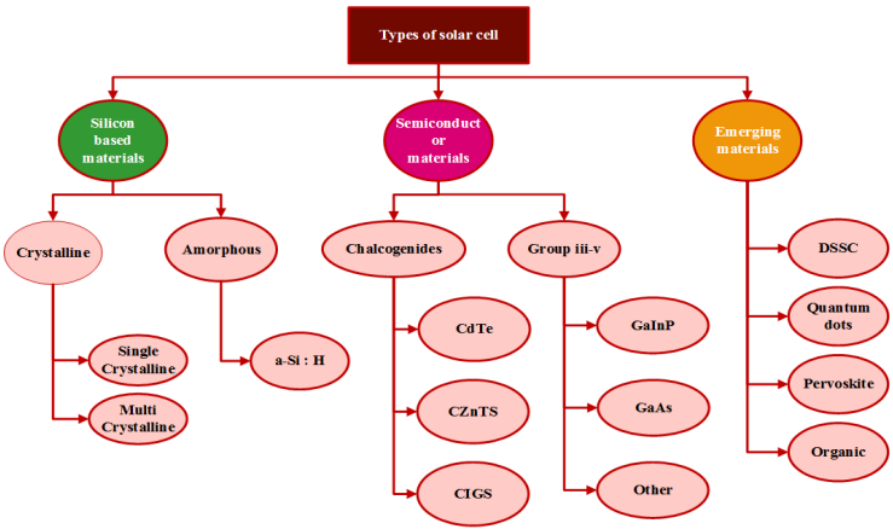

Fig. 2.1 Classification of solar cells technologies [31].

To effectively utilize the sun's energy using solar technology, homeowners and business owners can install solar hot water systems and design their buildings with passive solar heating in mind. In **Fig.2.1** solar cell technologies has been classified in three sectors.

Gallium arsenide (GaAs), copper indium gallium selenide (CIGS), and cadmium telluride (CdTe) are examples of thin-film solar cells. Organic photovoltaic (OPV), dye-sensitized solar cells (DSSC), and perovskite solar cells (PSC) are emerging solar cells. This type of solar cell has the advantages of being lightweight and inexpensive. However, there are significant issues that prevent them from being used on a big basis. Organic solar cells are still need to improve in terms of conversion efficiency [32]. The all-solid perovskite solar cell, which is based on DSSC but overcomes its drawbacks, drew a lot of attention from scientists as soon as it was announced.

Solar batteries, for example, store electricity and can be used during periods when solar production is low. Furthermore, solar-plus-storage solutions are suitable for all sizes of solar panel installations and offer numerous additional benefits, such as energy reliability, grid resiliency, and lower-cost power.

Solar energy has been used by mankind since the dawn of time, but it wasn't until the nineteenth century that the first attempt at photovoltaic energy was produced. Grid-connected solar systems did not begin to do substantial effort for generating suitable power until the early twenty-first century.

Over the last decade, the photovoltaic sector has exploded. Apart from growing public knowledge that the world's oil sources may run out in the not-too-distant future, photovoltaic technology development is also fueled by societal environmental concerns. Solar power generation, in this regard, is a potential generation of electric power with moderately low global warming gas releases across its whole life cycle.

An interface between p-type and n-type materials is formed as a result of the specific chemical potentials of electrons and holes across the interface, which provides a built-in electric field.

The low maximum efficiency can be attributed to two factors. The solar cell, on the one hand, does not absorb photons with an energy of E<Eg. Even electrons excited by photons with an energy E > Eg, on the other hand, can only supply the band gap energy (Eg) to the electric circuit, with the rest (E-Eg) being lost to thermal dissipation [10]. Photovoltaic cells can be

classified into three generations based on their theoretical maximum conversion efficiency and the nature of their materials. The first category contains cells that use high-purity materials with low levels of structural flaws. These are the most efficient cells available right now. As previously stated, crystalline silicon solar cells fall under this category having efficiency of 25% [33].

The percentage of solar energy shining on a PV device that is transformed into useable power is the conversion efficiency of a photovoltaic (PV) cell or solar cell. Improving conversion efficiency is a major research target that will allow PV systems to compete with traditional energy sources in terms of cost.

2.3 Dye-Sensitized Solar Cell (DSSC)

Dye-sensitized solar cells (DSSC's) convert solar energy into electrical energy. DSSC's initiate how plants harness solar energy. In a DSSC, electrons originate from a dye when it absorbs light. The dye contains a conjugated system (Alternating single and double bonds) that absorbs light in the visible spectrum, from the types of the solar cell we have seen that from the emerging materials of solar cell 'DSSC' is one of them.

2.3.1 History of Dye-sensitized Solar cell

DSSC is a p-n Junction photo voltaic devices. The light absorption and charge detachment processes are combined in DSSC by combining a sensitizer as a light-absorbing material with a wide band gap semiconductor. In 1970 it was disclosed that TiO_2 with a small bias voltage by exposing to light could split water [34]. So with the introduction of nano Porous TiO_2 electrodes, providing a huge active surface area and cell combining such electrodes and a redox electrolyte based on iodide/tri iodide couple upgraded the conversion efficiency to 7% in 1991. In the year of 2003 Ruthenium based dyes and polymer gel electrolyte with good thermal stability was used and 6% of gaining max efficiency [35].

The use of an iodide-based redox electrolyte resulted in an 8% efficiency in 2008. [36]. The researchers tried to fix the corrosive nature of the electrolyte, which aided in improving the photovoltaic efficiency and device stability upto 11.5% [37]. Considering the advantages and disadvantages of the first and second generation of PV technologies researchers have proposed quantum dot solar cell ($\eta = 10\%$); organic solar cell ($\eta = 11\%$); DSSC ($\eta = 13\%$); raised the third generation of solar PV. This 3rd generation technology is able to optimize efficiency with great reduction of the cost of the device.

Due to exceptionally low-cost material and mechanical flexibility; ease to fabricate and assemble as well as friendly, DSSC as a potential optional choice to solar PV generation have been able to draw the attention. The solar cell composed of a wide band gap of 3.2eV for TiO_2 is regarded as the most efficient material for the electron transporting material for DSSC. A good competitor of TiO_2 photo anode is ZnO though ZnO has higher electron mobility and electron diffusion coefficient. But the conversion efficiency of ZnO of 0.4%-5.8% is lower than that of TiO_2 of 11%. The band gap, electron transport times, and dependence of light intensity is similar for both ZnO and TiO_2, But electron lifetime is great for ZnO to compare to TiO_2 But "recombination rate" for ZnO is much lower than that of TiO_2. Besides TiO_2 is much efficient than ZnO. The synthesis of TiO_2 nanostructures namely "nanoparticle", nano rods (NRs) nanowire (NWs), nanotubes (NTs). The production of these structures of TiO_2 are done by several synthetic analysis such as sol-gel analysis, hydrothermal and solvothermal procedure, chemical or physical vapor deposition methods organic acid precursor method; electrochemical deposition method, etc.

Table 2.1 A comparison of Chemical, Electrical, Thermal, Mechanical and Optical Properties of TiO_2 and ZnO.

Properties		$\boldsymbol{TiO_2}$	$\boldsymbol{ZnO}$
Chemical Property	1.Crystal structure	Tetra gonal (Rutile Anatase, brookie)	Hexagonal (Rock Salt, Zinc Blende, Wurtize)
	2.Lattice Parameter	a= 0.3785 nm c= 0.951nm	a= 0.3249 nm c=0.52nm
	3.Band gap (ev)	3.2-3.59	3.2-3.3
Electrical property	4.Dielectric constant	114(Rutile)	8.5
	5.Electron effective mass (me)	9	0.24
	6.Electron diffusion coefficient [cm^2s^{-1}]	0.5(Bulk TiO_2), 10^8-10^4(np film)	5.2(Bulk ZnO)1.7×10^4(np film)
	7.Electron mobility Cm^2/Vs	Thin film :0.1-4.0	Thin film:205-300(Bulk ZnO)
Thermal Property	8.Thermal Conductivity ($Wm^{-1}k^{-1}$)	8.4	0.6,1-1.2

Mechanical Property	9.Density (g/cm^3)	3.79	5.606
	10.Melting point(C)	1875	1975
Optical Property	11.Refractive index	2.54	2

In this **Table 2.1**, the properties of TiO_2 nanostructures particularly for DSSC has been mentioned. This will show that the impact of photo electrode film with TiO_2 NP can magnificently increase the performance status of solar cells with a large area of absorption, easily photo-excited electron being delivered to transport path away directly impactful scattering center for enhanced light-harvesting efficiency. The advantage of choosing TiO_2 np as a working electrode over ZnO motivated me to proceed with more improvement in the conversion efficiency of Dye-sensitized solar cells.

In **Fig.2.2** development of solar cell has been shown where dye-sensitized solar cell is a promising photo electrochemical cell's efficiency of up to 13% and an optional method to Si-base solar cell. But despite having the same good advantages of DSSC, The maximum conversion efficiency compared to silicon is lower compared to a silicon-based solar cell.

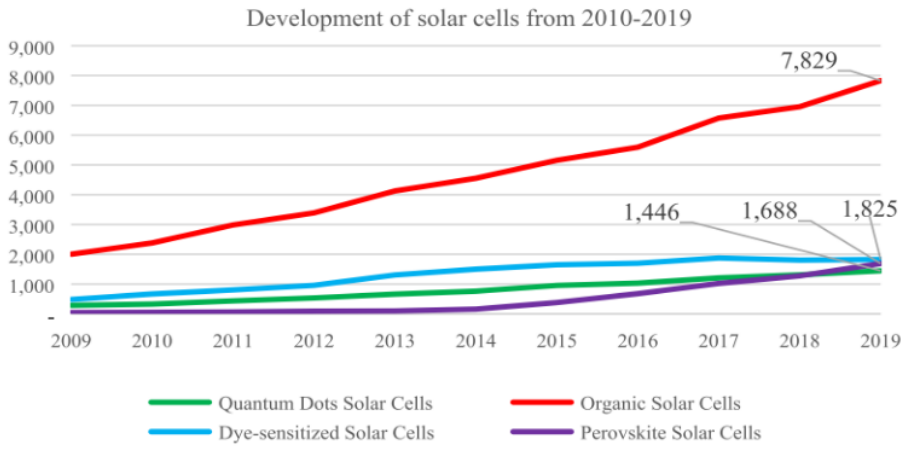

Fig. 2.2 Development of solar cell from 2010-2019 [2].

Because of their chemical quality, surface area for dye absorption, and proper energy band, TiO_2 nano particle film coated onto Fluorine doped tin oxide (FTO) layers used as photoelectrodes in DSSCs. Because electron transport in a nano particle network occurs via a

series of hops to adjacent particles, not all photogenerated electrons can reach the collecting electrode. The trapping process may reduce the efficiency and oxidized redox species if the thickness of TiO_2 increases. The recombination problem may be solved by using ZnO as an alternative. Because it has large exciton binding energy (60MeV). But the entire efficiency of TiO_2 DSSC's is higher than that of ZnO DSSC.

Because the effectiveness of ZnO thin passivation shell layers is lower than the highest recorded in TiO_2 DSSCs. So the dye absorption procedure is the primary issue with ZnO loss DSSC. Because of the high carboxylic acid binding group in the dyes, dissolution of ZnO and perception of dye Zn^{2+} complex occurs, resulting in low overall electron injection efficiency of the dye [38].

2.3.2 Factors affecting the efficiency of DSSC

- Working function and resistivity of FTO
- Semiconductor morphology and carrier transport properties (oxide material).
- Wavelength absorption and dye molecule-to-semiconductor-material interface alignment.
- Transfer of electrons from the Redox electrolyte to the stimulated dye molecule.
- The p+ counter electrode's catalytic interaction with the iodic electrolyte.

2.4 Basic Structure of DSSC

Components information of DSSC should be known well to understand how light energy is converted into electricity done by DSSC based on sensitization of wide band gap semiconductors. The basic components of DSSC's shown in **Fig 2.3** are consisted of the following things which play a vital role to improve overall efficiency by optimizing each of them. The Basic Components are

1. Photo sensitizer / Dye
2. Electrolytes
3. Photo electrode
4. The counter electrode (CE)
5. Conductive glass substrate

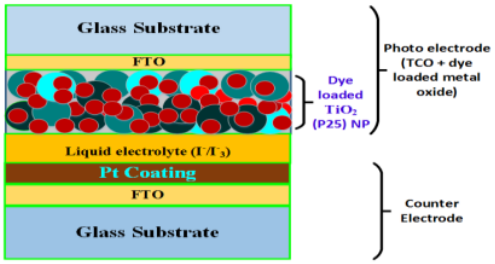

Fig. 2.3 Structure of DSSC.

2.4.1 Photo sensitizer / Dye

Dye has essential roles for the maximum absorption and conversion of solar to electric energy. An efficient photo sensitizer has several basic fabrications requires:

a) The dye needs to be luminescent
b) The absorption spectra of the dye should cover the ultraviolet-visible and near-infrared region
c) large visible light-harvesting capacity
d) Well, the injection of electron efficiency is the semiconductors conduction band.
e) $-O$ or $-OH$ groups with anchoring capability on TiO_2 surface ensuring High rates in the transfer of electrons.

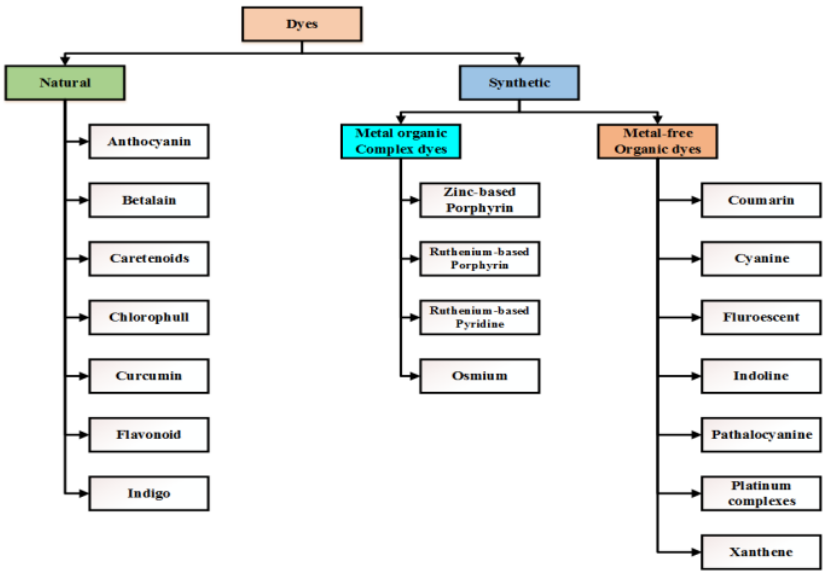

Fig. 2.4 Categories of common dyes used in DSSC with example [39].

Ru complex's photo sensitizers (N 719) for dye-based DSSC shows the highest efficiency of 11.2% By Gratzel and his group [40]. Because the absorption spectra of Ru complex dye cover ultra violet visible and near inferred region, Ru complex has the large visible light-harvesting capacity with good chemical stability and the possible exchange of charging with semiconductor solids. In **Fig 2.4** categories of common dyes of DSSC is shown.

2.4.2 Electrolytes

The Electrolytes make the transport of charge between the photo electrode and counter electrode with the presence of a redox mediator. five main components of an electrolyte such as I^-/I_3^- are 1) redox couple 2) solvent 3) additives 4) cations 5) ionic liquids [41]–[43].

The redox potential of the iodide/tri iodide should be addressed for dye and electrolyte regeneration. Iodide/tri iodide is successful redox couple used in DSSC. Iodide, iodides, and sometimes other additions make up a redox electrolyte.

The electrolyte has three types base on the solvent used for its preparation in DSSC. They are "Aqueous Electrolyte", "organic solvents based Electrolytes" and "Ionic liquids based Electrolytes" where Ionic liquids provide has long-term thermal and chemical stability excellent ionic conductivity. I^-/I_3^- has been shown as a high efficient electrolyte despite that I/I electrolyte erodes glass/ TiO_2/Pt [44], [45].

2.4.3 Conductive Glass or Substrate

Conductive oxide coated glass is not only used for photo anode but also used for (CE). The conductive glass should have an abundant supply, high optical for being employed as the substrate. The second is efficient charge transfer, which lowers energy loss in DSSC. TCO films are manufactured not only of fluorine doped tin oxide (FTO), but also of indium doped tin oxide (IDTO) (ITO). The film resistance of less than 20OΩ per sq at room temperature, considering between 10-20Ω per sq. This layer is coated for electrons emitted from the photo anode (dye coated TiO_2) to be collected and sent to the counter electrode via an outside circuit. As a result, it is known as a current collector.

2.4.4 Photo-Electrode / Working Electrode

On a Fluorine doped tin oxide (FTO), TCO glass substrate electrode or working electrode in DSSC is prepared by depositing a thin film layer of Nano structure semiconductor material. Such as TiO_2 , Nb_2O_5, ZnO, SnO_2 (n-type), and NiO (p-type) are sample conductor materials

are used for it. Among them TiO_2 is used widely for being Non-toxic, less expensive, and abundant material means easily available. The electrode appeared as transparent porous electrode film has the thickness from $10\mu m$ to $15\,\mu m$ and size of inter connected nanoparticle varying from $15 - 30\,nm$ of the formed porous electrode film.

Both screen printing and doctors' blade method are being used as the deposition technique for film preparation. The viscous TiO_2 paste which is coated onto the substrate is done by these two methods to involve the deposition of viscous TiO_2 paste. With the combustion for removing binder metal oxide (TiO_2) paste onto the substrate, The sintering is carried out of (450-500)℃ after the screen printing and doctors blade method for deposition of viscous colloidal TiO_2 on a substrate is done. TiO_2 as photo anode or working electrode to be the best semiconductor for having good efficiency and stability ZnO also shows better efficient photo anode, as it has a band gap close to TiO_2.

2.4.5 Counter Electrode

In DSSC structure counter Electrode plays a vital role. It is constituted with fluorine-doped tin oxide (FTO) glass with platinum (Pt.). The counter electrode influences photo voltaic parameters. The output voltage for the over the potential counter electrode that appears from the delivered current through electrolyte and electrolyte / CE interface for the full filament of redox reaction platinum paste is used for the counter electrode to reduce the tri-iodide to iodide after redox reaction counter electrode is important and formation of iodide for rege is important.

2.5 Working Principle of Dye-sensitized solar cells

A dye-sensitized solar cell means a solar cell that is sensitized by a Dye. “Dye” means light-sensitive material. “Light absorption”, “Charge Separation” and “Charge collection” are the processes involved in the working principle of DSSC. A simple flow chart regarding the working principle of DSSC is given below in **Fig.2.5** :

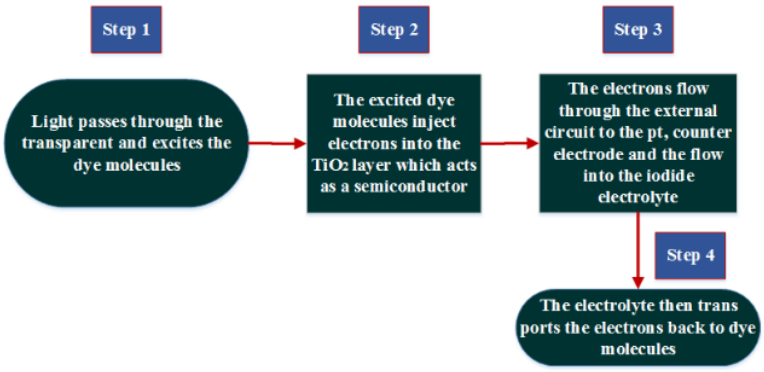

Fig. 2.5 Flow chart of basic Working principle of DSSC.

Working process:

The TiO_2 np is placed on the conducting electrode (photo-electrode) to adsorb sensitizers (dye molecules) Photons absorb dye molecules, which are stimulated from the Highest occupied molecular orbital (HOMO) to the Lowest unoccupied molecular orbital (LUMO) states. The redox electrolyte is linked to the monolayer of photo-sensitive dye and is in contact with the wide band gap oxide semiconductor. The oxide is injected with photo electrons, which are supplied by electron donation from the electrolyte, when an electron is introduced into the Conduction Band of a Semiconductor nano structured TiO_2 sheet with a wide band gap. The photo sensitizer (dye molecule) is oxidized. The injected electron (electricity) travels through the cell before being extracted and sent to the load, where the work is converted into electrical energy. TiO_2 nanoparticles serve as highways for the injected electron (electricity) to travel through the cell before being extracted and sent to the load. I-/I3- redox electrolytes occupy the gap between the Nano particles, and Ions are employed as an electron mediator between the TiO_2 photo electrode and the Pt. coated counter electrode. The oxidized dye molecules (photo-sensitizer) are therefore regenerated by accepting electrons from the I- ion redox medium tor.

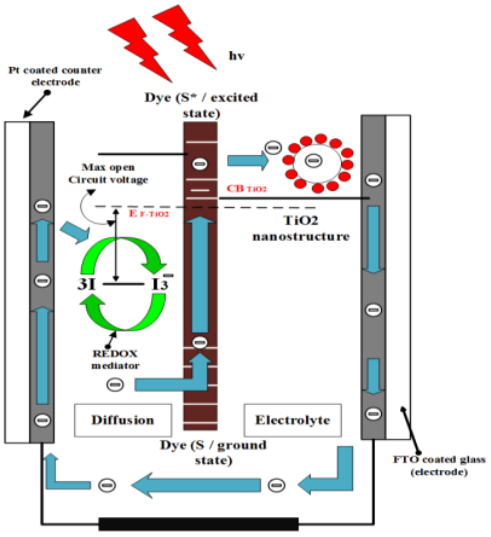

Fig. 2.6 Schematic representation of working principle of TiO_2 base dye-sensitized solar cell.

This whole procedure and components reaction have been shown in **Fig.2.6** and **Table 2.2** respectively.

Table 2.2 Component's reaction of DSSCs and process

SL No.	Reactions	Result
1	$TiO_2 \mid S + hv \rightarrow TiO_2 \mid S^*$	Excitation
2	$TiO_2 \mid S^* \rightarrow TiO_2 \mid S^* + e^- (cb)$	Injection
3	$TiO_2 \mid 2S^* + 3I^- \rightarrow TiO_2 \mid 2S + I_3^-$	Regeneration
4	$I_3^- + 2e^- (\mathrm{pt}) \rightarrow 3I^-$	Reduction
5	$I_3^- + 2e^- (\mathrm{cb}) \rightarrow 3I^-$	Reception (dark Reaction)
6	$TiO_2 \mid S^* + e^- (cb) \rightarrow TiO_2 \mid S$	Recombination (dark reaction)

2.6 Performance analysis of DSSC

As the world's population grows, so does the need for renewable energy. Solar energy is the most abundant and inexhaustible energy resource, and silicon solar cells have grown in prominence in recent decades as traditional energy sources have dwindled [46]. Because of

its easy construction methodology and low cost, dye-sensitized solar cells (DSSCs) are thought to have a significant promise in the field of photovoltaic [47]. For the effective creation of nonporous TiO_2 in the anatase phase, many synthesis methods have been used, the most frequent and simple of which are sol-gel, hydrothermal, and solution combustion synthesis techniques [47], [48].

Without considerable performance degradation, a photovoltaic device must be functional for 40 years. The conductivity of all elements of Nano crystalline injection solar cells, including the conducting glass, TiO_2 layer, sensitizer, electrolyte, the counter electrode, and sealant, has thus been carefully examined. The TCO glass and Nano crystalline TiO_2 layer are unquestionably stable, thus research has concentrated on the four other components [49]. When compared to the TiO_2-ZnO Nano composite-based dye-sensitized solar cell, the TiO_2 nanoparticle-based dye-sensitized solar cell had a higher current density[46]. The anatase phase of TiO_2 nanoparticles has a bandwidth of 3.2eV and has shown promise in DSSC applications [50]–[52]. Furthermore, as compared to TiO_2 nanoparticles, ZnO nanoparticles have a broader bandwidth of 3.3eV and greater excitonic electron mobility of about 115cm^2/V.S [49]. Chung et al. reported employing solution combustion synthesis to produce TiO_2 Nano powders with a specific surface area of 47m^2/g, which were employed in the production of DSSC [47]. Govindaraj et al employed a hydrothermal technique to make TiO_2 nanorods, which were employed as photoanodes in a DSSC and had a 5.42% efficiency [48]. Wahyuningsih et al used a mechanochemical approach to make TiO_2 NRs-ZnO composite and used it as a photoanode in a DSSC efficiency of 0.85 % [53]. Myrsini Giannouli et al synthesized nanostructured TiO_2 and employed it as a photo anode in a DSSC efficiency of 0.39%.

The photon-energy-to-electricity conversion efficiency is described as follows for solar spectrum radiation with photon flux:

$$\eta = \frac{J_{sc} \times V_{oc} \times FF}{J_0}$$

Here,

J_{sc} =short circuit current;

V_{oc}=open circuit voltage;

J_0=photon flux;

FF=fill factor;

In another way, kind find the performance. It is evaluated by power conversion efficiencies (PCE), Short-circuit current density, open-circuit voltage (V_{oc}), maximum power output [P_{max}], series and shunt resistance, incident photon conversion efficiency (IPCE) and Fill Factor (FF),

Different kind of dye for power conversion efficiency (PCE) were calculated in **Table 2.3**:

Table 2.3 Power conversion efficiency in different Nanostructures in TiO_2.

TiO_2 Nanostructure	Compounds	PCE (%)
Nanoparticles/ Nanotubes	N719 + AC-9 + CDCA	6.97
	N719 + AC-9	6.48
	AC-9	4.56
	N719	5.56
Nanoparticles/ Nanowires	N719 + AC-9 + CDCA	5.44
	N719 + AC-9	4.9
	AC-9	2.5
	N719	4.15
Nanoparticles	N719 + AC-9 + CDCA	6.69
	N719 + AC-9	6.1
	AC-9	4.21
	N719	5.1

Considering the tiny mistakes that show that the manufactured cells are very repeatable, just one device per type was produced with TiO_2 nanotubes and nanowire [54].

2.7 Photo electrode treatment for improvement of the performance

The creation of modern dyes is directly connected to the improvement of dye adsorption through the development of photo anodes. New photoanodes with increased dye absorption and charge transfer are being developed, while light photon absorption is being improved and electrons are being injected into the semi-conductor ducting line [54].

In the fast and novel, highly restructuring construction of a photoanode, exact comparison studies between cells using various TiO_2 nano-components are possible in the fuel cells. Using the combination of an innovative photoanode construction with a synthetic dye enables current DSSC constructions to be developed simultaneously. Due to their excellent efficiency and stability compared to other materials, TiO_2 is determined to be the best photoanode semiconductor. ZnO showed improved efficiency among the aforesaid metal oxides because it is nearer to the TiO_2 band gap and has discovered greater carrier mobility. The effective photoanode that may substitute for TiO_2 is thus found. But the recombination of photo-enthusiastic carriers and the ZnO surface volatility in the acid dyes constituted the biggest obstacle for ZnO to achieve high conversion efficiencies [31]. Researchers have attempted to enhance efficiency by changing structure, surface morphology, particle size, photoanode thickness, etc.

2.8 Overview of Titanium Oxide (TiO_2)

TiO2 is a semiconductor with exceptional optical and electrical characteristics, as well as cheap cost, non-toxicity, chemical, and thermal stability. That is why it is an effective photocatalyst. Organic pollutants are fully degraded by photocatalysis, which converts them to harmless CO_2 and H_2O. Many researchers have proposed ways to enhance TiO_2 's photoactivity in the UV and visible light spectrums.

2.8.1 Properties of Titanium Oxide (TiO_2)

TiO_2 has electrical, Chemical, and optical properties which are described below:

2.8.1.1 Electrical Property of TiO_2

The valence band (VB) of wide-gap rutile and anatase comprised of 'O' 2p states, where conduction band (CB) is formed by Ti 3d states. Electrical Properties like Electrical resistivity, Dielectric constant, Dielectric strength, Dissipation factor basically depend on the crystal's graphic direction. TiO_2 crystals have a high resistivity valve up to 10^{15} ohm-cm and

bulk oxygen vacancies, titanium interstitial, and reduced crystal surface are considered to generate shallow electron donor levels which approach the TiO_2's electron conduction. The ionization energy has been reported to 0.007eV to 0.08eV based on temperature for interstitials where oxygen vacancies as double donor helps in electron conduction. In high-temperature mobility reduce for the small polar diffuse by tunneling anatase TiO_2 shows higher electron mobility. However, in both anatase and rutile base, the crystal structure are high concentration of donors leads to the formation of impurity band.

2.8.1.2 Optical properties of TiO_2

Refractive index, UV transmittance, and Reflection co-efficient, etc. represent optical properties of TiO_2. In anatase because of the wide absorption band with its maximum in the IR the blue color has been observed from a source refraction index, UV transmittance, and Reflection coefficient is found 2.6, 10%, and 4.9 respectively [55].

2.8.1.3 Chemical Properties of TiO_2

The Chemical Properties of TiO_2 contains a chemical formula, Molecular weight (79.86g) crystal structure (Tetragonal). Lattice constant (a=4.5937 A), (C=2.9618A) from the crystal structure of TiO_2 we get three common polymorphs: Ruthie (tetragonal), Anatase (tetragonal); brookie (or thorium bic) along with TiO_2 II (columbite), TiO_2 III (baddeleyite) TiO_2 (B) (monoclinic), TiO_2 (H) (hollandite). Among them, Ruthie is most stable, where Anatase is inmate stable phase based on room temperature and transforms irreversibly into Rutile with threshold temperature around 1Kc.

2.8.2 Application of TiO_2

TiO_2 has several applications; some of them are given below:

a) In construction material.
b) for pigment application.
c) Oil spill application.
d) In waste treatment.
e) In soil application.
f) In air purification and water application.
g) Ceramic glaze.
h) Electronic data storage media.

i) Energy conversion (solar cell).

j) Water splitting (Hydrogen evaluation).

k) Residence exterior (painting/Tile, Glass/Tent).

2.9 Parameters of Anatase and Rutile structure of TiO_2

At ambient circumstances, titanium oxide crystallizes in four different structures: a) Rutile, b) anatase, c) brookite, and d) srilankite [56], [57]. The most stable structure of TiO_2 is rutile [58]. Basic physical parameter of TiO_2 is described in following **Table 2.4** [55], [59]–[61].

Table 2.4 Physical properties of TiO_2

No. of Physical parameters	Physical and structural parameter's name	Anatase	Rutile
1	Crystal structure	Tetragonal	Tetragonal
2	Energy Band gap (eV)	3.23-3.59	3.02-3.24
3	Refractive index	2.54, 2.49	2.79, 2.903
4	Solubility in HF	Soluble	Insoluble
5	Solubility in HO	Insoluble	Insoluble
6	Hardness (Mohs)	5.5-6	6-6.5
7	Bulk modules (GPa)	183	206
8	Density (g/cm^3)	3.79	4.13
9	Lattice parameters (nm)	a= 0.3785 c= 0.9514	a= 0.459 c= 0.295
10	electron mobility [cm^2/Vs]		Crystal= 0.1-10 Thin film= 0.1
11	Molecular weight (g/mol)	79.88	79.88
12	Melting point (C°)	1825	1825
13	Boiling Point (c)	2500-3000	2500-3000
14	Specific gravity	3.9	4.0
15	Light absorption (nm)	$\lambda \leq 385\ nm$	$\lambda \leq 415\ nm$

16	Dielectric Constant	31	114
17	Ti-O Band length (A°)	1.965 (2)	1.980 (2)
18	Average Particle diameter, nm	50	50
19	Thermal Conductivity ($Wm^{-1}K^{-1}$)	8.4	8.4
20	Specific heat ($JKg^{-}1K^{-}1$)	692	692
21	Electron effective mass [me]	9	
22	Electron diffusion coefficient [cm^2s]	0.5 (bulk TiO_2) 10^8-10^4 (nanoparticle film)	
23	Dielectric Strength	4-8 kv/mm	
24	Dissipation Factor	0.00020-0.0050	
25	Reflection coefficient	0.49	

2.10 Synthesis of TiO_2 nanomaterial for DSSC

It has been discovered that when the size of a material shrinks, new physical and chemical characteristics emerge at the nanoscale scale.

In these types of nanomaterial of TiO_2, the abundant form of TiO_2 offers better surface area to volume ratio because the size of the TiO_2 material is now at nanometer scale helps to successful dye adsorption size of the material [62], [63]. Nanoparticles, nanorods (NRs), nanowires (NWs), and nanotubes (NTs) are all types of TiO2 nanomaterials that are synthesized using different techniques [64]. In our investigation, for TiO_2 based DSSC, Ruthenium (Ru, N719) dye is used. **Table 2.5** and **Table 2.6** shows synthesis method and nanostructure and efficiency report of TiO_2 respectively.

Table 2.5 Synthesis methods of TiO_2

Chemical Method	Physical Method
1) Sol-gel method	1) Thermal decomposition
2) Micelle and inverse	2) Plasma arcing
3) Condensation method	3) Sputter deposition
5) Sol method	4) Evaporative deposition
6) Hydrothermal and solvothermal method	5) Pulse laser deposition
	6) Electron beam physical vapor deposition
	7) Cathodic arc deposition

Table 2.6 TiO_2 Nanostructures and Obtained efficiencies from literature reports.

Group	Material / Method	Isc (mA/cm^2)	Voc (V)	FF	Eff (η) (%)
Sun et al.,	P25 nanoparticles chemical synthesis	5.04			2.70
Yun et al.,	P25 nanoparticles chemical synthesis	9.50	0.79	0.74	5.62
Hamadanian et al.,	P25 nanoparticles chemical synthesis	16.40	0.72	0.55	6.56
Alam Khan et al.,	P25 nanoparticles chemical synthesis	22.30	0.67	0.43	6.59

De Zhao et al.,	P25 nanoparticles chemical synthesis	5.86	0.64	0.70	6.33
Marco et al.,	P25 nanoparticles chemical synthesis	11.30	0.70	0.70	5.50
Niu et al.,	P25 nanoparticles chemical synthesis	12.55	0.75	0.6	5.80
Hao et al.,	P25 nanoparticles chemical synthesis	12.84	0.77	0.66	6.59
Agarwala et al.,	P25 nanoparticles chemical synthesis	7.60	0.70	0.67	4.0
Xu et al.,	P25 nanoparticles chemical synthesis	8.90	0.72	0.66	4.25
Fan et al.,	Nanorods hydrothermal synthesis	4.56	0.75	0.71	2.45
Pan et al.,	Nanorods hydrothermal synthesis	4.08	0.67	0.34	0.93
Guo et al.,	Nanorods hydrothermal synthesis	2.57	0.63	0.47	0.76

Koo et al.,	Nanorods sol gel synthesis	4.08	0.67	0.34	0.93
Yang et al.,	Nanorods Microwave synthesis	2.65	0.85	0.60	1.31
Guang et al.,	Mesoporous hydrothermal synthesis	16.67	0.74	-	8.20
Wang et al.,	Mesoporous microwave synthesis	15.60	0.60	0.53	5.0
Kim et al.,	Mesoporous sol gel synthesis	16.03	0.72	0.50	5.88
Hou et al.,	Mesoporous chemical synthesis	13.03	0.71	0.56	5.31
Jung et al.,	Mesoporous hydrothermal synthesis	13.2	0.73	0.72	6.99

2.11 Advantages and limitations of TiO_2 based DSSC comparing with ZnO-based DSSC

Because of its outstanding properties, titanium dioxide, often known as titania, is the semiconductor of choice for dye-sensitized solar cells (DSSC).

In our investigation, TiO_2 np is used as the liquid electrolyte in DSSC. TiO_2 has a strong ionic character that shows that as constituted of Ti^{4+} and O^{2-} ions which have been observed in Electrophoretic deposition analysis of TiO_2 deposition.

2.11.1 Reason for TiO_2 is used for DSSC

1. TiO_2 has a suitable band.
2. TiO_2 is used for High dye loading.
3. It has high electronic mobility for collecting electrons with photos generated [64].

2.11.2 Advantage of TiO_2 over ZnO based DSSC

Comparing to ZnO it has "high charge collection efficiency" and more "electron transportation that makes as good electrode while fabricating a typical DSSC" photoconversion efficiency of ZnO-based DSSC as limited moreover Zn^{2+}/dye complex in acidic dye shows low performance compared to TiO_2 based DSSC. Besides lower injection efficiency with Ru- based dyes. In ZnO shows the electron injection is controlled by slow component whereas in TiO_2 electron injunction is controlled by fast component. In TiO_2, the conduction band is mostly made up of vacant Ti^{4+} 3d orbitals where the ZnO conduction band is presented from the empty s and p orbital of Zn^{2+}. Because ZnO's chemical stability is significantly lower than that of TiO_2, its dye adsorption properties are severely limited.

2.11.3 Limitation of TiO_2 on DSSC

Electron carrier mobility of ZnO (115-155cm/vs) is higher than that of the electron mobility of TiO_2 (10-5cm/vs) and ZnO can be doped in both n-type and p-type. Scientists discovered that ZnO has a lot of promise and can help cells operate better. The Density of state value is found to be more for Zincite in the valance band region compare to TiO_2.

2.12 Alternative of TiO_2

All of them were employed as part of the often researched TiO_2 periods, like anatase, rutile, and brookite in DSSC's photo anode. When contrasted to rutile and brookite, the anatase phase possesses features such as an indirect band gap, which does not encourage direct electron transition from conduction to the valence band, and hence gives an order of magnitude longer lifespan for photo-generated electrons. In addition, the photo generated transporter's reported recombination in anatase is somewhat less as the effective mass of photo carriers that can help their rapid migration is reduced [65].

A variety of methods are used to increase TiO_2 characteristics within the visible electromagnetic spectrum range: (a) metal and nonmetal implantation; (b) iota implantation;

(c) composite with other halving machines quantum dot sensitization; (d) TiO_2 sensitizing synthetic and/or natural organic dyes with physical and/or chemical adsorption.

Titanium oxide is known to have been utilized frequently in solar cells as an n-type oxide of the metal. Highly poisonous, strong electron mobility, visible wavelength range, high transparency, adequate transmission range, cheap cost, high chemical stability, and wide range are the major reasons.

The energy gaps of these oxides are 3–3.2eV. Also, encouraging results have been obtained by other wide-band oxides such as ZnO and Nb_2O_5. TiO_2 is utilized mostly as a semi-conductive layer since it is non-toxic and less costly and its simple availability [66]. The efficiency is still poor compared with silicon solar cells in TiO_2-based Dye-Sensitized Solar Cell [67]. DSSC employs natural dyes at a rate of around 0,89%, whereas silicon solar cells with an efficiency of roughly 20% [68]. Low efficiency is caused by a large quantity of free electron recombination with oxidative dye molecules.

The restriction of electron transport in TiO_2 layers produces significant levels of recombination. Low electron transport is due to lower optimum particle interaction. In addition, electrons trapped on this grain boundary offer increased possibilities for recombination [19].

2.13 Scale-up and Commercialization of DSSC

The expansion and industrial trends of the global population will provide a huge problem in the near future to address the growing energy consumption. In comparison to high-cost conventional silicon solar cells, dye-sensitized solar cells are widely recognized as low-cost photovoltaic devices due to their low-cost materials and simple fabrication process. Dye-sensitized solar cells are made up of titanium oxide (TiO_2) semiconductor, which is frequently used as a paint basis in the pigment industry, and a dye sensitizer, which may be derived cheaply from a range of natural resources. Carbonic materials might also be utilized to replace platinum catalysts that can down material costs further. The DSSCs are straightforward to produce as they are insensitive and process able at ambient temperature to environmental pollutants. In roll-to-roll processes, a continual cheap production technique for printing color-sensitive solar cells on flexible substrates is chosen for these unique properties. In addition, even under darker situations, such as dawn and dusk or overcast weather, DSSCs

can operate better. DSSCs are a great choice for interior applications such as windows and sunroofs because of their efficient utilization of diffusion light [69].

The performance of photovoltaic should be the figure of merit that finish derived as

$$\frac{energy\ conversition\ efficiency\ \times lifetime}{true\ costs}$$

Here, true costs include production, supply, and establishment expenses as well as environmental effects. From this value number and a set of additional assumptions, other values may be derived, such as leveled power costs. Manufacturing of DSSC products has begun in earnest, with cell efficiencies above 12.2%, demonstrations of steady performance over several years, and low-cost production methods. Dozens of businesses and industrial research labs are currently active in the development, marketing, and manufacture of DSSC technology and products, mostly in Europe, Asia, and Australia. In **Table 2.7** applied area of DSSC is shown

Table 2.7 Development of commercial based DSSC in different countries.

Companies	Types of application
G24 Innovations (G24i), Wales (2009)	First to commercialize a DSSC product.
Tata Stee, Dyesol (Australia)	Largest DSSC modules (over $1m^2$), DSSC materials and equipment, building-integrated photovoltaic.
3GSolar, Israel	DSSC modules for off-grid rural applications.
Aisin Seiki (Toyota Central R&D Laboratories), sony, sharp	Large area solar panels power generation and indoor electronics
SJC-Shimane Inst. of Industrial Tech.	Street lights and road signs
Sony's self-powering lamp shades	Consumer household electronics

More information on the approximately 25 businesses working in DSSC research, development, and commercialization can be found here. Recent advances in increasing the efficiency, stability, and manufacture of DSSCs give insight into potentially successful research avenues for overcoming remaining problems in these areas. Among the research areas are fundamental scientific examinations of DSSC materials and interactions, material

development and discovery, and efforts to improve the integration of DSSC cells into modules and panels via inline manufacturing. In many cases, increasing efficiency means sacrificing stability and manufacturability, and vice versa. The compromises achieved will be decided by the DSSC application's specific requirements [70].

2.14 Preparation of photo-electrode of DSSC

Four important parameters of a DSSC are the working electrode, sensitizer (faring), redox-mediator (electrolyte), and counter electrode. A mesoporous layer of oxide, made up of Nanometric particles and monolayers of color adhered to the surface which cause light absorption, is a photoelectrode. It is a crucial part of DSSC because photons are converted into electricity. Dye electrons initially get stimulated from the higher occupied molecular orbital (HOMO) to the lowest unoccupied molecular orbital (LUMO) when exposed to sunlight. The electrodes of the photograph are created by depositing a finely layered oxide semiconductor on transparent conduction glass plates composed of FTO or ITO [40]. An electrolyte solution consisting generally of an iodide/tri-iodide redox pair gives electrical ions to renew the oxidized color. Lastly, the electrodes carry the tri-iodide ions back to the iodide through the external circuit and to complete the process. Great electron injections, good electron collecting, and good use of light are believed to be good photo-electron. Many other materials were investigated in DSSCs as photo electrode. The low recombination rate for the hole-electron pair and high absorption feature is most frequently employed in TiO_2 (titanium dioxide powder) [71].

One key prerequisite for making an effective DSSC is to produce a homogenous layer of photo electrode. In DSSC, the photo electrode consists of semiconductor material for the nanostructure, which is clipped onto a transparent supporting material. TiO_2 is the most often utilized semiconductor material as it is a cheap, non-toxic, and plentiful substance. The electrode consists of linked, 15-30 nm long, nanoparticles. They seem like a translucent porous electrode, averaging 10-15µm in thickness. Screen-printing and doctor bubbles are the deposition processes used largely for film preparation. Before a sintering operation, viscous colloidal TiO_2 is placed on a substratum. Sintering is usually done at 450-500° C. Sintering. The high temperature leads to electric interconnections between the nanoparticles and ultimately generates a porous electrode nanostructure. Dye sensitization is done by immersing the electrode for some time in a dye solution.

2.15 Electrophoretic Deposition (EPD)

Electrophoretic deposition (EPD) is a colloidal technique used in ceramic manufacture that offers the following advantages: quick formation time, simple apparatus, no substrate shape restriction, and no mud for binding burn out because the green coating includes few or no organics [72]. In EPD techniques preferred liquid is organic, Required conduction of liquid medium is low, no charge transfer on deposition and moving species are solid particles [73]. EPD has four steps [74]. These are-

a) **Dispersion.**
b) **Electrochemical charging**.
c) **Electrophoresis**.
d) **Deposition**

from various deposition techniques for thin film deposition, these technologies are classified into four processes [75].

Namely-

1) Eva's positive process.
2) Glow Discharge process
3) Gas-phase chemical process
4) Liquid-phase chemical processes.

Where in **Table 2.8** liquid phase chemical processes has been shown

Table 2.8 Liquid-Phase chemical Processes

Electro processes	Mechanical Techniques
Electroplating	Spray pyrolysis
Electroless plating	Spray on techniques
Electro lytic anodization	Spain On techniques
Chemical reducing plating	
Chemical Displace	
Electro phoretic Deposition	

2.15.1 Introduction of Electrophoretic Deposition

Electrophoretic Deposition encompasses a variety of industrial techniques such as electrocoating, cathodic electrodeposition, anodic electrodeposition, and electrophoretic coating. Electrophoretic deposition (EPD) uses the concept of electrophoresis to move and deposit colloidal particles floating in a liquid medium onto electrodes.

2.15.1.1 Principle of Electrophoresis

Electrophoresis is a method molecule moves to an electrode of opposite charge Molecules with positive charge move towards "cathode" and negative molecules move towards Anode. "Charge on the molecules" and potentially applied across the electrodes leads to the migration. The rate of migration depends on particle net charge, weight size, shape, and applied electric current when electricity is given molecules base on their charge moves to their respective electrodes. These molecules' migration for different speeds and length depends on their charge, mass, and shape. The procedure is shown in **Fig 2.7.**

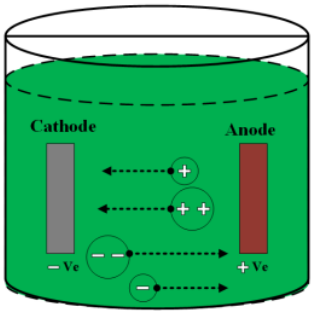

Fig. 2.7 Schematic diagram for Principle of Electrophoresis.

2.15.3 Factors influencing EPD

Charge particles in a suspension are deposited onto an electrode under the influence of an applied electric field in the EPD process.

Two groups of parameters shown in **Table 2.9** determine the characteristics of this process-

1) Suspension based parameters
2) Process based parameters

Table 2.9 Parameters governing EPD

Suspension based parameters	Process based parameters
i. Zeta potential.	i. Applied voltage.
ii. The dielectric constant of liquid.	ii. Effect of deposition time.
iii. Stability of suspension.	iii. The concentration of solids in suspension.
iv. Particle size.	iv. Effect of deposition distance.
v. The viscosity of the suspension	
vi. Conductivity of suspension	

2.15.4 Types of Electrophoretic Deposition (EPD)

The electrophoretic Deposition process has two important types, these are

a) Cathodic Electrophoretic Deposition (EPD)
b) Anodic Electrophoretic Deposition

2.15.4.1 Cathodic Electrophoretic deposition:

Following the process of electrophoresis technique, with a particular applied electric field, the positively charged material is attracted to the cathode electrode for deposition. In this analysis cathodic electrophoretic deposition is performed on TiO_2 solution.

2.15.4.1.1 Working principle of cathodic electrophoretic deposition for TiO_2 solution

From the principle of Electrophoresis, it has been seen that when a molecule is charged positively then it move towards the cathode due to charge on molecules and potentially applied across the electrodes. Since the purpose of using cathodic electrophoretic deposition is to deposition of the positively charge ion of TiO_2 where we see

$$TiO_2 \rightarrow Ti^{4+} + 2O^{2-}$$

from **Fig. 2.8** the positively charge Ti^{4+} of TiO_2 solution move's toward cathode/FTO, a glass substrate for deposition with the particular applied electric field and there is a certain distance is being made between two electrodes that are how the cathodic Electrophoretic deposition is done which leads to getting a uniform to creak free TiO_2 layer on conductive glass substrate based on DSSC application.

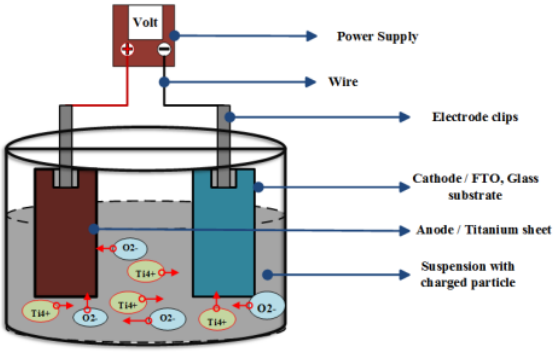

Fig. 2.8 Cathodic Electrophoretic Deposition for TiO_2 solution.

2.15.4.1.2 Advantage of Cathodic Electrophoretic Deposition

a) Corrosion protection at a high level is applicable
b) Staining and other problems occur at anode because of oxidation, which is neglected in the cathodic EPD process.

2.15.4.2 Anodic Electrophoretic Deposition

With the process of electrophoresis technique, when an electric field is applied all of the negatively charged molecules migrate toward or deposited on the positive charge electrode or anode which is shown in **Fig.2.9**.

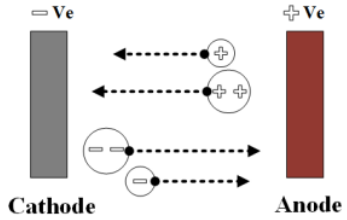

Fig. 2.9 Schematic diagram of Anodic EPD.

2.15.4.2.1 Advantage for Anodic Process

a) Anodic process in terms of cost is lower than that of cathodic process.
b) Control requirement for this process is not complicated
c) Varying the substrate quality shows less sensitivity.

2.15.5 Application of Electrophoretic Deposition

1. In oriented ceramic materials, EPD is used for fabricating crystalline oriented thick films, Textured TiO_2, Alumina,
2. For Multilayered compositions such as Multilayered alumina, TiO_2 is used
3. In DSSC application
4. For Piezoelectric materials (PZT actuators)
5. EPD is used for producing coatings for shaping monolithic, laminating objects, and infiltrating porous materials.

2.16 Multilayer Electrophoretic Deposition

In order to develop the performance and Efficiency of the Dye-sensitized solar cell (DSSC), the Electrophoretic deposition method has achieved wide attention in DSC's technology. For the preparation of homogenous coated layer, controllable conditions, and binder-free process, EPD synthesis has several advantages [76],[77]. More than ever before EPD can readily install nano-partical film in one step, with controlled film thickness, enabling multi-component site-selective deposition, and no restrictions on substrate form, for example. advantage provided by EPD has enhanced the use of EPD in fabrication for DSSC [3][4][78][79].

But eventually, the fact that the EPD technique is facing a problem regarding the thickness of the layer is creak formation. Due to the contraction of thin films, the evaporation of leftover solvents can cause creak. The newly formed creaks, which can be been clearly by eyes result in poor electron transport characteristics and a reduction in dye load on the TiO_2 surface. And that's why the heat treatment and thickness of the prepared films play a vital role in the TiO_2 structure and overall efficiency of DSC's. Many methods such as, "using a mixture of TiO_2, fiber and nanoparticles, mechanical compression of titania-nanoparticle film and as binder using TiO_2 / polymer blend have been reported to decrease the creaks in EPD films but these applications are limited for creak reduction of EPD. To achieve the uniform and precise and compact full deposition Electrophoretic deposition of TiO_2 has been inquired by many researchers [80][81][82]. But the researchers are concerned about the non-uniform and having a huge amount of creaks for the TiO_2 layer. That is why the multilayer deposition technique has been introduced in the previous work for which we are investigating [83]. from single-layer deposition to three-layer deposition followed by EPD technique show a huge amount of crack in FTO glass substrate by seeing in SEM image. Although with the

increasing deposition layer is followed by a significant change of parameters related to EPD such as a) effect of deposition distance b) applied voltage, c) effect of deposition time. The crack of the thin film of TiO_2 has been found reducing. In our investigation, we have seen from the previous work that, to improve the quality of the TiO_2 layer two effective multilayer deposition techniques have been introduced, they are

a) conventional multilayer (Cathodic Electrophoretic deposition, 4LD)
b) Modified Multilayer (4L4SEPD technique).

2.16.1 Convention multilayer (Cathodic EPD)

Conventional multilayer is basically a four-layer deposition technique where the substrate position is kept some. This multilayer deposition technique with four different steps shows the huge crack reduction in the prepared layer at glass substrate compared to one step, there step TiO_2 layers respectively with changing the parameters regarding deposition mentioned in earlier.

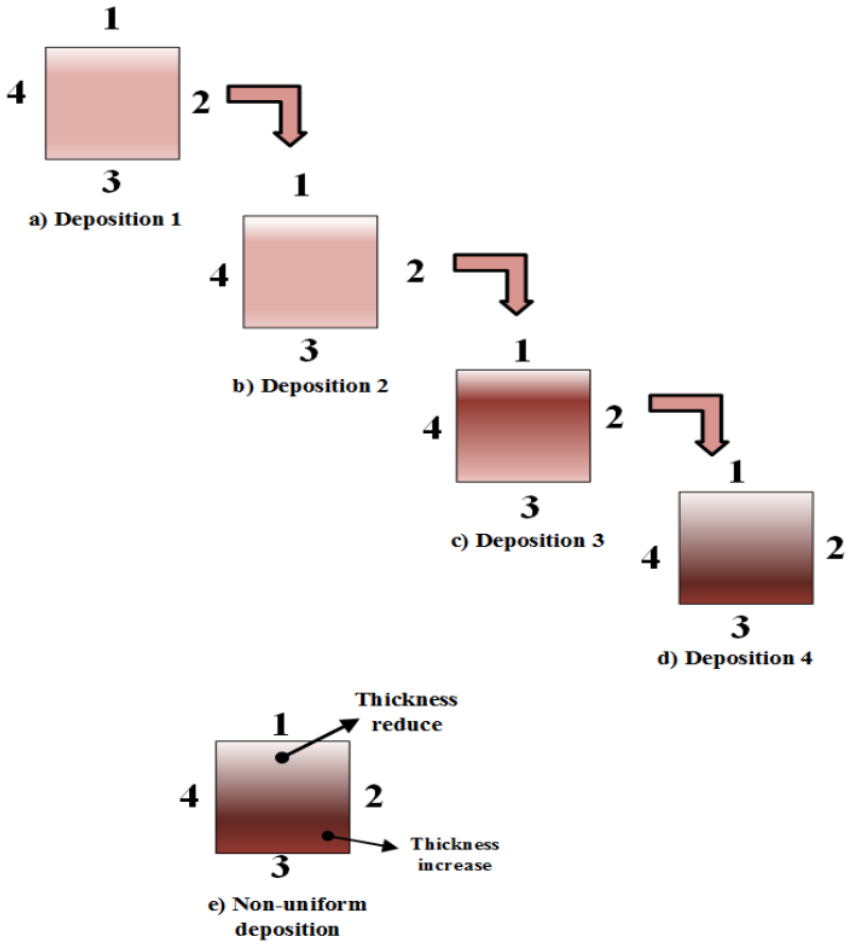

Fig. 2.10 Four-layer EPD (a-d) where $2 \times 2cm^2$ substrate's position is the same and (e) shows the non-uniform deposition substrate.

In **Fig. 2.10** we have observed that if the side of the substrate position is not changed in 2*2 cm substrate which shows in **fig (e)** of figure 2.10 that the thickness in one side get decrease and one side increase which shows that from this conventional multilayer EPD technique we won't get "uniform" deposition referred from previous work [83]. This means it gives a Non-homogenous layer.

2.16.2 Modified Multilayer EPD (4L4S EPD)

The problem produced in four-layer cathodic EPD that is the non-uniform deposition of the substrate has been improved by a four-layer four side electrophoretic deposition system.

Where uniform deposition of the substrate has been achieved. In **Fig 2.11** the substrate position is changed in each deposition. It has been found that if the deposition is done by rotating the side of the substrate four times, we get a uniform deposition of the substrate fig (e) which leads to improving the quality of the TiO_2 layer, increase the efficiency of the layer, and as well as the layer becomes more compact than previous deposition technique.

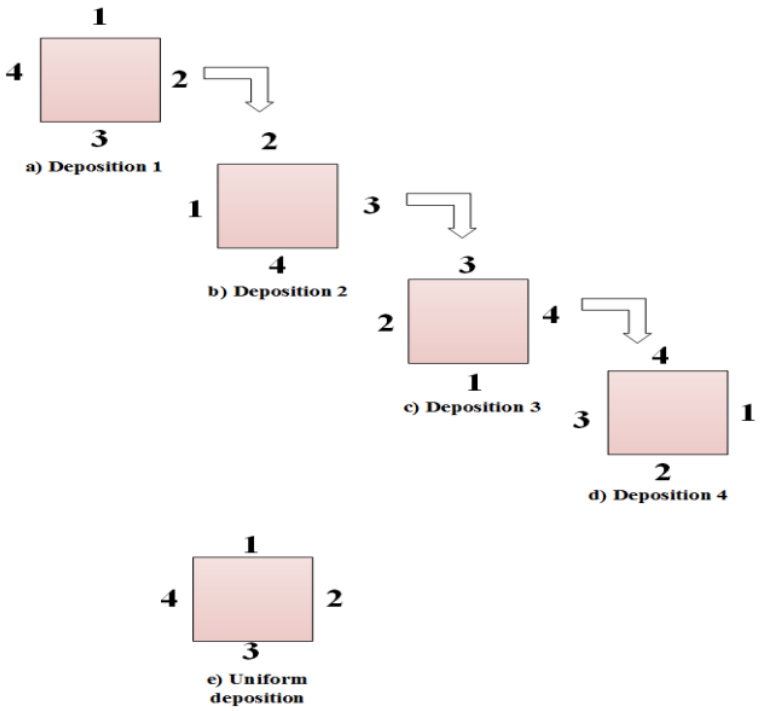

Fig. 2.11 4 layer 4 Side EPD (a-d) where substrate position is changed and (e) shows uniform deposition substrate.

2.16.3 Advantages of Multilayer Electrophoretic deposition

i. Creak on the substrate gets reduced compared to single-layer deposition.
ii. The layer becomes more compact.
iii. The efficiency of the layer gets increased greatly.

2.17 Compression and Hot compression in DSSC

An effective photoanode allows good light collecting and electron transmission in DSSC applications. The electron carrying mesoporous oxide layer binds the dye molecules in the

photo anode and gathers the photo generated electrons from the dye's excited state. According to another piece of literature, an efficient electron transporting layer should have a large surface area to increase dye loading for effective light harvesting, be transparent to visible light to reduce incident photon loss, and have a conduction band below the (LUMOs) of the dye to allow sufficient injection of photo generated electrons. In the photo, a hope the microstructure, particle size, porosity, and pore size distribution of the semiconducting particles play important roles to modulate the photovoltaic characteristics [84].

The photoanode is prepared by TiO_2 nanoparticles due to its chemical stability, non-toxicity, relatively high transmittance in the visible spectra. Reducing electron sports paths is done by reducing thickness. Different post-deposition treatment (compression, hot compression) has been used in nanoparticle material to enhance the layer's quality or to transport more electron in deposition process to increase photovoltaic characteristics and efficiency of dye-sensitized solar cell by characteristics structures and morphologies of TiO_2, ZnO, using field emission scanning electron microscope (FE-SEM). Also with the study of electrochemical impedance spectroscopy to quantify the light-harvesting efficiency and the charge transport impedance at the various interface in DSSC.

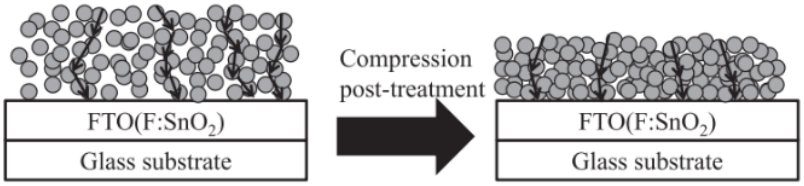

Fig. 2.12 Doctor blade method for deposition of TiO_2 [24].

In **Fig 2.12** mechanical compression of TiO_2 deposited film has been shown. Among various deposition techniques "Hot compression" with the help of EIS analysis is being utilized to observe the effect of compression pressure and temperature on the electron transport phenomenon. Applying compression pressure at a higher temperature (130MPa, 70°C) offers improved P-V performance when utilizing hot compress for ZnO based DSSC, according to prior research [29],[85].

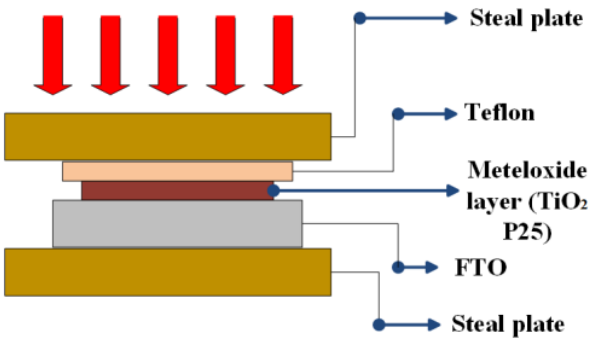

Fig. 2.13 Schematic diagram of compression arrangement.

Fig. 2.14 Compression machine and temperature variation mini test press -10

In our investigation, though the EPD method has been used to make the layer of TiO_2 np more compact with uniform deposition with using hot compression technique in a compression machine mini test to showed in **Fig 2.14** TiO_2 np has been compressed to improvising surface quality and also varying the temperature of compression plate shown in **Fig 2.13** performance gets change significantly. So application of hot compression with EPD gives a more homogenous and compact layer to improves the overall efficiency as the photovoltaic performance of DSSC.

2.18 Electrochemical Impedance Spectroscopy (EIS)

In order to characterize the electrical properties of materials and their interface, impedance spectroscopy is an effective method [86]. The immense boost of (EIS) has taken it to a significant level in the field of DSSC. It is mostly used to assess the material's electrical characteristics as well as its interactions with surface-modified electrodes [87]. Electrochemical impedance spectroscopy (EIS) is a reliable method for determining the current response when an ac voltage is applied as a function of frequency. EIS is highly successful at employing modest ac voltage amplitudes that cause very little system disturbance. EIS has been widely used to investigate the kinetics of electrochemical and photoelectrochemical processes, including the clarification of important electronic and ionic processes in DSSC, as well as electrochemistry, biomedical applications, material science, and other fields [88].

AC is another name for EIS. Impedance spectroscopy can discriminate between dielectric and electric characteristics of individual contributions to the components under examination. J.Ross Medonold reveals the EIS for measuring the impedance using AC polarography inducing electrochemical reaction for low amplitude sinusoidal oscillation as a function of frequency. The electrochemical cell has been used to estimate the dielectric properties of meat inspection, milk, leather's quality checking, evaluate electrical properties of drinks, and water which was being reported earlier. In solid and liquid electrolytes. Impedance investigations including the mobility of ion vacancies and interstitials, ionic conducting glasses and polymers, fused salts, and nonstoichiometric ionically banded single crystals have all been employed in EIS.

IS is used to study dielectric materials such as solid or liquid nonconductors having dipolar rotational electrical characteristics, as well as materials that predominantly conduct electricity [89]. Summary of the Impedance spectroscopy's application are:

1) Characterization of material including the microstructural model of materials for impedance spectra, layer modeling, modeling of composite electrodes with several experimental techniques.
2) Characterization of the Electrical response of high resistivity ionic and dielectric solid materials by emittance spectroscopy.

3) In solid-state devices related to solid electrolyte chemical sensors, photo electrochemical solar cells, Impedance response of Electrochemical material and device, etc.
4) Corrosion of materials.
5) Electrochemical power sources.
6) Batteries and fuel cells (Alkaline fuel cell. polymer Electrolyte fuel cell, solid oxide fuel cell).

To evaluate the impedance data, Impedance spectroscopy has become a key technique for studying the characteristics and quality of dye-sensitized solar cell systems. Impedance spectroscopy has brought revolutionary changes. IS provides the basic strategy of operation of solar cells in order to release interpretation of the experiment result by discussing the basic photovoltaic principles. In order to understand how 'IS' is applied in DSSC regarding modeling, measurement, and interpretation highlighted by the author's experience, we need to understand How it appeared and at the same time involved over the first years. In 1990, a large internal area carried by nanostructured Titanium oxide (TiO2) semiconductor, linked to a transparent conducting oxide (TCO), and covered with photoactive dye molecules became the "standard" configuration DSSC. It's also in touch with a redox I-/ I3-an electrolyte, which is linked to a Pt-catalyst counter electrode (CE). The DSC was designed to be a photo electrochemical solar cell at first. To examine the electronic and ionic processes in the DSSC, electrochemical impedance spectroscopy (EIS) was used. The major problem in the DSSC in our study is the interfacial charge transfer between a solid conductor, the working electrode (WE), and an electrolyte, primarily liquid electrolyte. This is accomplished by applying a voltage between WE and CE in the presence of a reference electrode (RE), allowing for the detection of the voltage drop at the electrolyte-working electrode interference. The electrolyte frequently contains salt, which gives it a high conductivity in the liquid phase and allows it to move freely in an electrical field. The interfacial charge transfer functions regulated by reactant diffusion are the subject of electrochemistry. EIS can easily distinguish between interfacial capacitance and charge transfer resistance, as well as determine the diffusion component in the electrolyte. Gabrielli gave a stable and effective introduction to such application at that time in 1991. Admittance spectroscopy (AS), a frequently used frequency technique in the solid-state, is a method that operates at the reverse voltage and assesses the energy level of majority carrier traps as well as state trap densities [90].

Representation of EIS

The data EIS may be present by present by

1) Bode plot (log z or Q as a function of log f)
2) The Nyquist or cole-cole plot, A typical EIS spectrum

Two or three semicircle shapes are attributed to impedance linked to charge transport at the pt counter electrode at TiO_2/ dye/ electrolyte and carrier transport by ions inside the electrolyte in the Nyquist plot for DSSC.

This implies that the charge transfer of TiO_2 / dye / electrolyte is connected to the central Arc in the mid-frequency band, based on the figure. The electrochemical reaction at the Pt counter electrode is represented by the higher frequency arc to the left of the center arc, while the lower frequency arc shows the I / I warburg diffusion process. So the overall impedance of the DSSC is the sum of the impedance at the Pt electrode, the impedance owing to tri-iodide diffusion in the electrolyte, and the impedance characteristics of the TiO_2 electrode. In order to extract meaningful information from impedance spectra, it is common practice to fit them with appropriate equivalent circuits or differential equations.

Since impedance is defined as the AC equivalent of resistance and is thus connected to alternating potential and current through ohms law, it is represented in ohms (Ω).

$$E\,(t) = |E_o| \sin(wt)$$

$$I(t) = |I_o| \sin(wt)$$

$$Z\,(w) = \frac{E\,(t)}{I(t)}$$

In a typical EIS experiment, the modulation frequency is sampled across a large range for a given potential, then the tiny modulation amplitude (E) is applied, resulting in the following:

$$E\,(t) = E_{applied} + |E_o| \sin(wt)$$

collecting data is then interpreted using a variety of plots. At a certain frequency f, the E(t) may have a different phase and amplitude than that of I(t) depending on the nature of the charger transfer process in the system that results in impedance of the corresponding charge transfer process- In general impedance is expressed by

$$z(w) = |z|(\cos \emptyset + j \sin \emptyset)$$

$$= zRe + jzim$$

$$\text{or, } z = z' + z'',\ Z' = |z| \cos\theta,\ z'' = |z| \sin\theta$$

16

$z'$and z'' are real and imaginary part of impedance respectively.

and phase angle,

$$\theta = \tan^{-1}\left(\frac{z''}{z'}\right)$$

$$\text{magnitude } |z| = \sqrt{(z')^2 + (z'')^2}$$

18

EIS data can be shown by Nyquist plots. Another method of graphing EIS data is the Bode plot. In **Table 2.10** Impedance representation is shown

Table 2.10 Impedance representation

Denomination	Definition	Real and Imaginary part
Impedance	$z(w)$	$z' + z''$
Phase angle	$\tan\delta = \frac{z''}{z'}$	
Complex dielectric constant	$\varepsilon*(w) = \frac{LC*(w)}{A}$	$\varepsilon* = \varepsilon' + \varepsilon''$
Complex dielectric modules	$M*(w) = \frac{1}{\varepsilon(w)}$	$M* = M' + M''$

EIS (electrochemical impedance spectroscopy) is a flexible and powerful analytical method for time-dependent processes in solution and at the liquid/solid interface.

Bearman, Boschloo, Hagfeldt then ascribed the internal behavior while charge flows through titania to the presence of such traps state later with the parameters related to EIS, are used to further evolution of DSSC using different post-deposition treatment method too. In **Table 2.11** advantages and disadvantages of EIS is shown.

Table 2.11 Advantage and disadvantages of EIS

Advantage	Disadvantage
1. Useful on High resistance material.	1.Expensive
2.Time-dependent data is available.	2.Complex data analysis for quantification.
3.Non-destructive	
4.Quantitative data available.	

2.19 Extension and formation of the work

In order to recognize the basic parameters, different types of properties, advantages and limitations of TiO_2 based DSSC comparing with ZnO-based DSSC analysis of EIS is important. These general objective leads the work to know the following thing-

1) The influence of Electrophoretic deposition on liquid electrolyte (TiO_2 np) on the glass substrate to make a homogenous uniform layer.
2) To improve the efficiency of TiO_2 based DSSC by post-deposition technique by making the layer more compact full.
3) Influence of the semiconductor morphology on TiO_2 based DSSC

CHAPTER 3

EXPERIMENTAL STUDY

3.1 Introduction

Application of mechanical compression at an elevated temperature (hot compression) is used for TiO_2 nanoparticle thin film, reduces the thickness. The preparation of flexible TiO_2 based photo anode is done using "four-layer-four-side-electrophoretic deposition (4L4SEPD)".Application of mechanical compression for glass substrate is a challenging matter due to fragile nature of the glass substrate .Thus very few literatures can be found where mechanical compression has been applied for glass substrate. In this investigation very low level of mechanical compression (only 40 MPa) has been applied with various temperature.

3.2 Experimental

The whole experimental section showing in **Fig 3.1** can be divided as follows-

a) **Cell fabrication**.

1. photo electrode preparation using four layer four side EPD.
2. Post deposition technique.
3. Dye loading.
4. Complete cell fabrication.

b) **Characterization**.

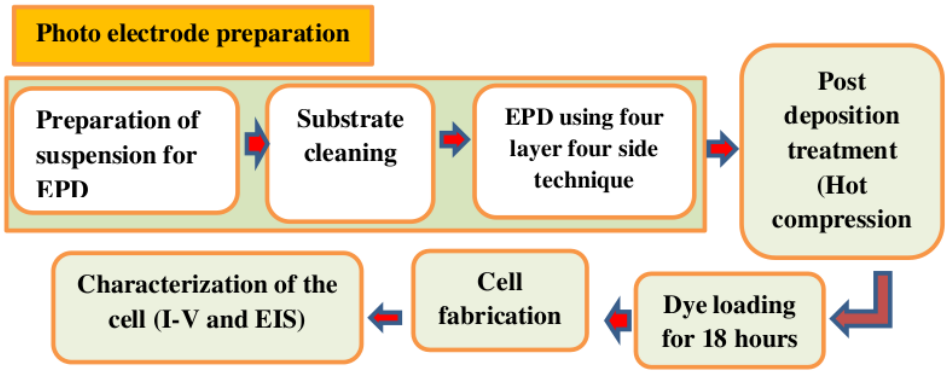

Fig. 3.1 Flow chart of experimental section.

3.2.1 Cell fabrication

1. photo electrode preparation using four layer four side EPD

Mixing 0.5 g of P25 TiO_2 powder, 0.1 ml of acetyl acetone, and 10 ml of H_2O with 100 ml of ethanol has been used for preparing the Suspension for EPD. To achieve a well-mixed suspension, a homogenizer (Sonic VCX-130) was employed to distribute TiO_2. Substrates cleaning process has been done using acetone (two times), and by methanol (one time) and dried N_2 flow and UV−O_3 cleaning. FTO glass substrate (2×2 cm^2, 15 Ω sq-1) and titanium-sheet (2×2 cm^2) have been used as cathode and anode respectively. At a distance of 2.5 cm, a pair of electrodes were vertically submerged in the suspension. Films were deposited by applying 30 V cm-1 DC field. TiO_2 acquires a positive surface charge in presence of H_2O and therefore, it goes towards the cathode. There was a tendency of depositing more TiO_2 particle at the lower portion of the substrate. Therefore, 4 layer 4 side deposition (4L4SEPD) techniques have been approached to ensure uniform layer photo electrode. One of the major challenges in the deposition of TiO_2 layer is the crack. At lower thickness the crack is very few. If the thickness increases, the formation of crack also increases which is not good for cell. Thus, four layer four side deposition techniques ensure a crack free layer up to a certain thickness level. The deposition is done on the FTO (Fluorine doped tin oxide) substrate.

2. Post deposition technique

The main purpose of using mechanical compression is to obtain a compact layer photo electrode. However, it is really very challenging to use mechanical compression for glass substrate photo electrode. In this investigation, a compressed machine (Mini TEST Press-10) with a very low level of mechanical compression (40 MPa). The compression was given by varying the temperature of the compression plate from room temperature to 90℃ . The optimum level of compression temperature was found about 70℃.

3. Dye loading

The fabrication and the characterization part has been conducted in Soga Lab, Nagoya Institute of technology. The whole experimental investigation has been conducted by Dr. M. S. H. Choudhury [83]. Here, electrode has been sensitized with Ru complex dye N719 at room temperature for 18 hours.

Complete cell fabrication

A sandwiched type solar cell was assembled by placing Pt-coated glass as a counter electrode above the dye loaded photo electrode in contact with iodide/triiodide redox electrolyte. A polymer film (Himilan) of 50μm thick was inserted between the electrodes. The active area of the cell was 0.16 cm^2 and thickness of the film was (12 - 14)μm.

3.2.2 Characterization

The characterization section has been done by M. S. H. Choudhury in Soga Lab, Nagoya Institute of Technology, Japan. The fabricated cells have been characterized using scanning electron microscopy image, Electrochemical Impedance Spectroscopy Analysis and Current-Voltage analysis using a solar simulator. The photovoltaic properties were measured using a solar simulator (100 $mW.cm^{-2}$, AM 1.5 illumination) in air with the area of 0.16 cm^2 restricted by a still mask. Surface morphology of the TiO_2 electrodes was observed using a scanning electron microscope (SEM). EIS has been analysis by the data from LCR meter.

CHAPTER 4

RESULT AND DISCUSSION

4.1 Introduction

In this section, the features regarding DSSC (with deposition) of dye-loaded TiO_2 P25 are being interpreted elaborately. These important features are given below:

1. Scanning Electron Microscopy (SEM).
2. Electrochemical Impedance Spectroscopy Analysis.
3. I-V curve analysis.

EIS analysis has been done with the following things:

i. Nyquist Plot.
ii. Bode phase Plot.
iii. Impedance (z'& z'') vs. log F plot.
iv. Dielectric Effect.
v. Electric module effect.
vi. Dielectric loss tangent vs. log f.
vii. Capacitance vs. log f effect

Of TiO_2 (P25) Nanoparticle-based dye-sensitized solar cell.

4.2 Impedance Spectroscopy Calculation

Calculation of impedance spectroscopy is shown in **Table 4.1**

Table 4.1: Calculation for Impedance Spectroscopy

	Rs(Ω)	$R_{ct}(CE)$ **(Ω)**	$R_{ct}(AE)$**(Ω)**	f_{max} **(s^{-1})**	μ **(cm^2/V_s)**	τ_{eff} **(ms)**
WTO	68.04	14.93	245.20	1000	4.79E-5	0.16
Compression at RT	72.12	10.26	122.62	794.30	3.04E-5	0.20
Compression at 50T	72.08	15.58	105.54	630.95	2.34E-5	0.25
Compression at 70T	72.12	9.79	47.88	501	1.79E-5	0.32
Compression at 90T	75.11	14.34	93.44	794.30	2.84E-5	0.20

R_s = From figure and the Excel value.

$R_{ct}(CE)$ = Diameter of the first semi − circle.

$R_{ct}(AE)$ = Diameter of the second Half semi − circle.

f_{max} = Peak point of the semicircle at lower frequency range.

$\mu = cm^2/V_s = \frac{eD}{K_bT} = \frac{eL^2}{K_bT\,\tau}$ = Electron mobility.

τ = Time constant or lifetime of electron at cirtain interface.

e(electron charge) = 1.60218E − 19.

L^2 = Thickness of the film.

K_b = Boltzman constant = 1.3806E − 23.

T = 273 + °C.

$\tau_{eff} = RC = 1/(2\pi fmax)$

4.3 Scanning Electron Microscopy (SEM)

Scanning Electron Microscopy (SEM) was used to see the surface morphology of P25 TiO_2 electrodes. A profilometer (Alpha – Step 500) was used to examine the thickness of the film.

SEM images of photo electrode's surface at different temperature Compression:

Compressed temperature has great influence on changing the surface quality of photo electrode. Here, **Fig. 4.1** shows the SEM image of the photo electrode's surface that has been changing with the increasing of different compression temperature. In **Fig. 4.1(a)** the surface quality of photo electrode has not been improve due to the absent of compression temperature to the decrease the pore in the film. But with the increasing of Comp. temperature varying from RT to 70°C (**Fig. 4.1(b), Fig. 4.1(c), Fig. 4.1(d)**) crack has been minimized as pores are been Comp. and reduce at Comp. temperature the surface quality of the photo electrode has been found more compact than that of others but at 90°C Comp. in **Fig. 4.1(e)** draw back has been found in the surface of the photo electrode.

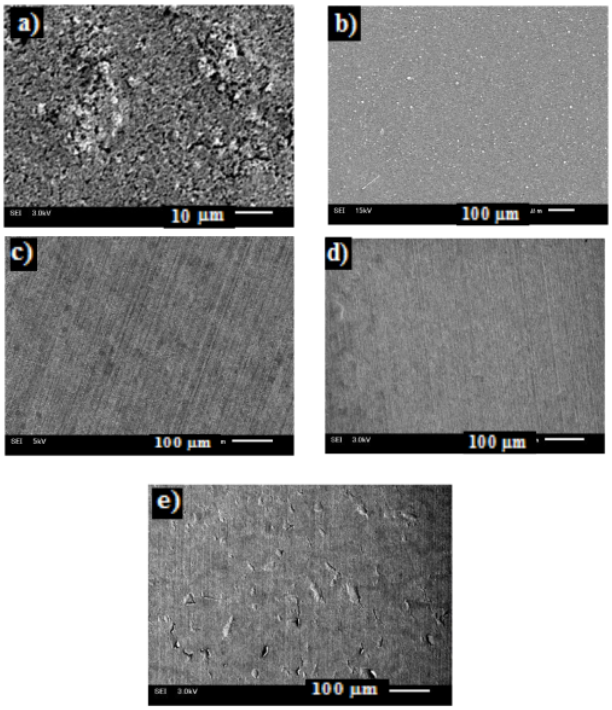

Fig. 4.1: SEM of the films (a)without Comp. (b) Comp. at Room temperature (c) Comp. at 50 °C (d) Comp. at 70 °C (e) Comp. at 90 °C [83]

4.4 Electrochemical Impedance Spectroscopy (EIS)

EIS is widely used as a standard characterization technique for many material systems and applications. This is a powerful tool in corrosion and solid-state laboratories. Analysis of a DSSC,s EIS spectrum reveals various critical charge transports, transfer, and build-up mechanisms in the cell. Related to DSSC's it permits a simultaneous characterization of the different processes taking place in the cell [91]. EIS is a steady-state technique for determining the current response to an ac voltage as a function of frequency. In EIS experiments, a tiny amplitude sinusoidal modulation per tubs the solar cell's potential, and the ensuing sinusoidal current response is measured as a function of the modulation frequency [92].

Almost everyone knows about the concept of electrical resistance. The meaning of electrical impedance can be understood starting from the concept of resistance. It is the ability of a circuit element. To resist the flow of electrical current from Ohm's law we get,

$$\text{R (resistance)} = \frac{V\,(voltage)}{I\,(current)}$$

Though it's a well-known relationship, its use is limited to only one circuit element the ideal Resistor. But the real world contains circuit elements the simple concepts force vs. to abandon the simple concept of resistance because these circuit elements exhibit much more complex behavior. Impedance resists the flow of Electrical current but unlike Resistance, it's not limited by the simplifying properties of an ideal resistor.

Electrochemical impedance is usually measured by applying an AC potential to an electrochemical cell and then measuring the current through the cell. The measurement of electrochemical impedance is normally done by applying a sinusoidal potential excitation (a small excitation signal). It is done so that the cell response is a pseudo-linear system, when a sinusoidal potential is applied to the system the current response to a sinusoidal potential will be a sinusoid at the same frequency but shifted in phase. The raw data for all measured frequencies in EIS experiments comprises of the real and imaginary components of potential difference E' and E'' and the real and imaginary components of current I' and I'' respectively. The phase shift (θ) and total impedance (Z) are the two basic parameters calculated out of the raw data using the following equation,

$$|Z| = \frac{V}{I} = \sqrt{R^2 + X^2}$$

$$R_s = E_s R = \|Z\| cos\theta.$$

$$X = \|Z\| sin\theta$$

$$C_s = \frac{1}{\omega x}$$

For data analysis purposes, the calculated impedance characteristics are expressed as magnitude and Nqauis plot (on a complex plane) and phase vs. frequency (Bode plot).

4.4.1 Nyquist plot

The EIS method consists of measuring the response of an electrode to a sinusoidal potential modulation at different frequencies. Analysis of a DSSC's EIS spectrum reveals various critical charge transport, transfer, and build-up mechanism in the cell. EIS analysis has been done using Nyquist plot with two semicircle. This plot also emphasizes circuit components that are in series. Here two interface resistance have found from the Nyquist plot. One is interface resistance between Pt. electrode and electrolyte represent as $R_{ct}(CE)$ and second one is the interface resistance between TiO_2 dye and electrolyte represent as $R_{ct}(AE)$. $R_{ct}(AE)$ Reflects the Warburg diffusion process of I^-/I_3^- [93]. It is appeared to be significantly delayed or almost overlapped with a semicircle at a higher frequency range due to the liquid electrolyte and this spear film. The parameters which are gained from the calculation and also explained in our previous report and how these parameters are changed with the application of different hot compression of post-deposition treatments [83].

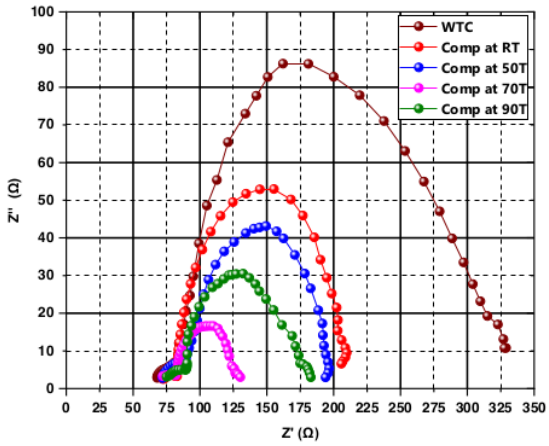

Fig. 4.2: Nyquist plot for TiO_2 based DSSC Prepared at different post deposition treatment (Hot Comp.) at (a) Without Comp. (b) Comp. at RT, 40 MPa (c) Comp at 50℃, 40 MPa (d) Comp. at 70℃, 40 MPa (e) Comp. at 90℃ at 40 MPa.

In **Fig 4.2** the values of R_s. are found to be Similar and $R_{ct}(CE)$. is also not so charge for all the simples. But $R_{ct}(AE)$ was significantly decreasing from 245.20Ω to 47.88Ω by the application of comp. at RT, comp. at 50℃, and comp. at 70℃ respectively.

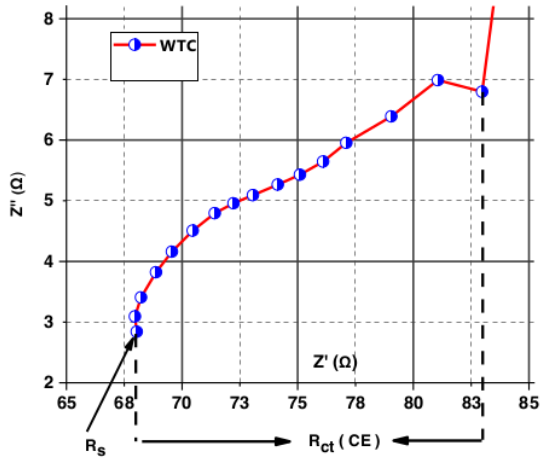

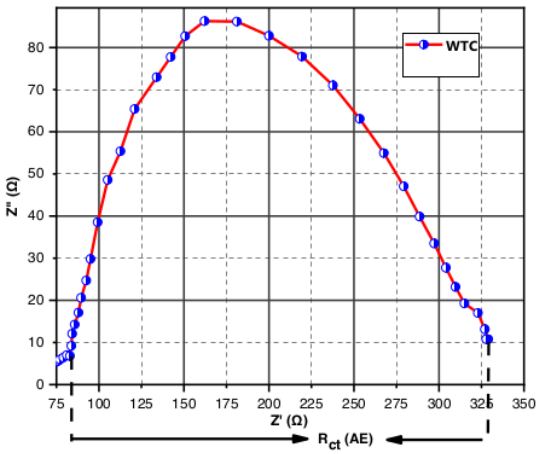

Fig. 4.3 : Value of R_s,$R_{ct}(CE)$, $R_{ct}(AE)$ in Nyquist plot of TiO_2

based on DSSC prepared without Comp.

In **Fig. 4.3** we see the impedance plot where the first and second semicircle is visible where 'R_s' was calculated from the first semicircle. So R_s value is the starting point at the first semicircle $R_{ct}(CE)$values are the difference between starting and ending point of the first semicircle and $R_{ct}(AE)$ value is the difference between starting and ending of the second semicircle. F_{max} is determined at the peak point of the second semicircle.

4.4.2 Bode Plot

Bode plots are another method for inter prating electrochemical impedance data and they consist of displaying $|Z(\omega)|$ and phase angle ($\emptyset$) versus logω. Here in this Bode phase plot, the characteristic frequency f_{max} (low-frequency peaks) is used to an estimated lifetime of electron (τ) using [29], [94]

$$\tau = \frac{1}{2\pi f_{max}}$$

This shows an inverse relationship between (τ) and F_{max}. The result regarding bode plot, the relation between V_{OC} and lifetime (τ) of the electron has been in an earlier report that is [29], [94]

$$V_{oc} \propto \ln \frac{1}{\tau_n}$$

In **Fig. 4.4** effect bode phase plot of the TiO_2 based DSSC prepared at different post-deposition (Hot compression) is shown. The characteristic frequency peaks of the charge transport (f_{max}) has been shifted toward lower frequency (from 1000 to 794.3s-1) by applying hot compression at room temperature and from (1000 to 630.95 s^{-1}) 50°C compression, (1000 to 501 s^{-1}) at 70°C compression and (1000 to 794 s^{-1}) at 90°C compression. The lifetime of (τ) inside TiO_2 electron was determined by the characteristic frequency (f_{max}) at low-frequency peaks. Layer electron lifetime (about 0.318ms) was obtained for the cell prepared with hot comp. at 70°C than the cell prepared with comp. at RT (0.2ms); cell prepared with comp. at 50°C (0.252ms); cell prepared with comp. at 90°C (0.2ms) which indicated the increasing rate of an electron lifetime from (0.2ms to 0.318ms).

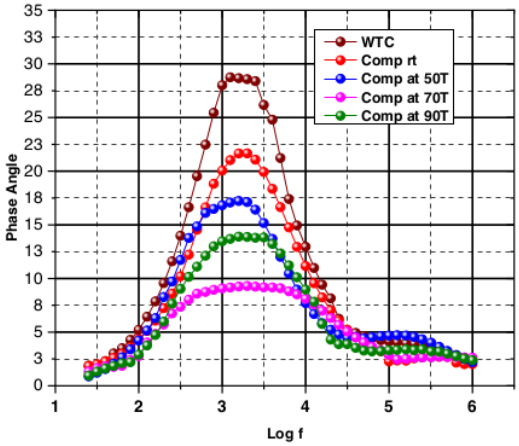

Fig. 4.4: Bode phase plot for TiO_2 based DSSC Prepared at different post deposition treatment (Hot Comp.) at (a) Without Comp. (b) Comp. at RT, 40 MPa (c) Comp. at 50°C, 40 MPa (d) Comp. at 70°C, 40 MPa (e) Comp at 90°C at 40 MPa.

4.4.3 z' vs. log F and z'' vs. log F

The real and imaginary impedance components will be affected by the material qualities of the electrode and the ionic properties of the electrolyte. To understand the impact of frequency over complex impedance and imaginary parts of the impedance against frequency

(log f) has been observed for five post-deposition (hot compression) in **Fig. 4.5** and **Fig. 4.6** respectively from the Figure for both $\boldsymbol{z}'$ and $\boldsymbol{z}''$versus log f, two different slopes for these five samples are visible. At the initial stage, from **Fig.4.5** we see the frequency dependence of the real part of the impedance $\boldsymbol{z}'$at low frequencies, the real part of the impedance $\boldsymbol{z}'$ has higher values. It decreases with increasing frequencies gradually. The decrease in trapped charge density and increase in charge carrier density can be attributed to this progression. At high frequencies, the merging of $\boldsymbol{z}'$ supports the presence of space charge in the material [95]. The $\boldsymbol{z}'$ vs. log f plot is suitable to evaluate the relaxation frequency of most resistive component [96]. The charge transfer resistance varied from (0.025 to 40kHz) at lower frequencies whereas at higher frequencies, all five resistances were nearly identical. At the lower side $R_{ct}(CE)$ is the charge transfer process interfacing platinum (pt) counter electrode and electrolyte. This charge transfer resistance for counter electrode remains' almost steady for the five samples. Or for all five cells. The electron transfer resistance at large semicircle from Nyquist plot at mid-range frequency represents the metal- oxide/ dye/ electrolyte interface resistance and is found to be different for different post deposition (hot compression) treatment for all five cells. For compression at RT to compression at 90°C. The $R_{ct}(AE)$ was found to be lower state gradually.

In **Fig. 4.6** the frequency and imaginary part of the impedance $\boldsymbol{z}''$ is shown where the spectrum is characterized with the peak at a frequency known as relaxation or characteristic frequency (f_{max}) which is related to electron life time [29], [94]. In Figure 4.8 the imaginary part $\boldsymbol{z}''$ at initial increase with the increase of frequency until it reaches a maximum peak of $\boldsymbol{z}''$ max then again starts to decrease for increasing of frequency since this imaginary part is a capacitive reactance and it is seen from this Figure that (f_{max}) decreases while applying hot comp. at RT (1000 to 794.3 s-1) at applying 50°C compression (from 1000 to 630.93s-1) at applying 70T compression (from 1000 to 501s-1) and at applying 90T compression (from 1000 to 794 s-1). Post deposition treatment.

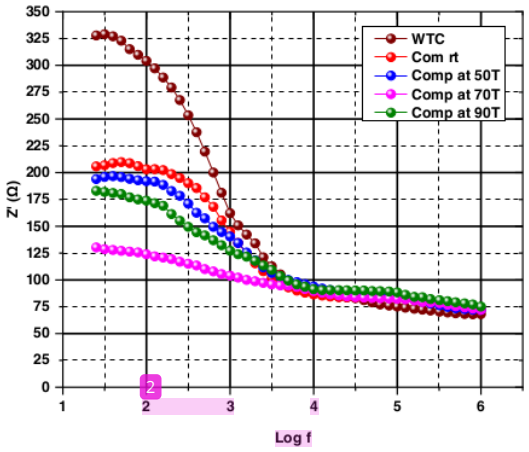

Fig. 4.5 : Variation of z' with $log\ f$ for TiO_2 based DSSC Prepared at different post deposition treatment (Hot Comp.) at (a) Without Comp. (b) Comp. at RT, 40 MPa (c) Comp. at 50℃, 40 MPa (d) Comp. at 70℃, 40 MPa (e) Comp. at 90℃ at 40 MPa.

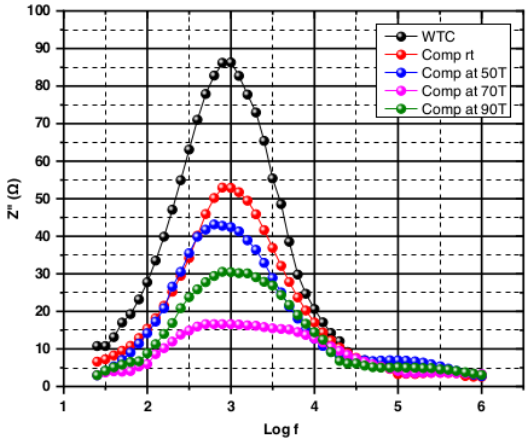

Fig. 4.6: Variation of z'' vs. $log\ f$ for TiO_2 based DSSC Prepared at different post deposition treatment (Hot Comp.) at (a) Without Comp. (b) Comp. at RT, 40 MPa (c) Comp. at 50℃, 40 MPa (d) Comp. at 70℃, 40 MPa (e) Comp. at 90℃ at 40 MPa.

4.4.4 ε' vs. log F, ε'' vs log F

To understand the conductivity behavior of electrolyte, the dielectric analysis makes an impactful effect regarding this The complex permittivity function ($\boldsymbol{\varepsilon}$ *) has two parts one is known as dielectric constant corresponds to energy store in material, and the imaginary $\boldsymbol{\varepsilon''}$ the part known as dielectric loss corresponds to dissipated energy. The complex permittivity function ($\boldsymbol{\varepsilon}$*) is a material property depending on temperature, the structural identity of the electrolytes, and the frequency of the applied field [97].

$$\varepsilon' = \frac{z''}{\omega C_o(z'^2 + z''^2)}$$

$$\varepsilon'' = \frac{Z'}{\omega C_o(z'^2 + z''^2)}$$

Where,

C_o = Vaccum Capacitance = $\frac{\varepsilon_o A}{t}$

ε_o = Free space permittivity = $8.85 \times 10^{-12} Fm^{-1}$

A = Area of electrode

t = sample thickness.

ω = angular frequency = $2\pi f$

f= applied field frequency

ε' = Real part of dielectric constant

ε'' = imaginary part of dielectric loss.

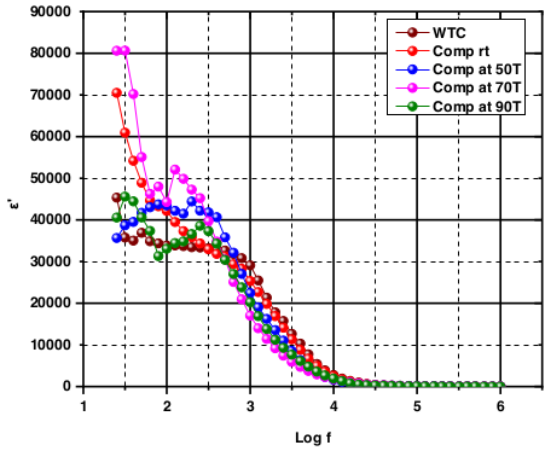

Fig. 4.7 : ε' vs. $log\ F$ for TiO_2 based DSSC Prepared at different post deposition treatment (Hot Comp.) at (a) Without Comp. (b) Comp. at RT, 40 MPa (c) Comp. at 50℃, 40 MPa (d) Comp. at 70℃, 40 MPa (e) Comp. at 90℃ at 40 MPa.

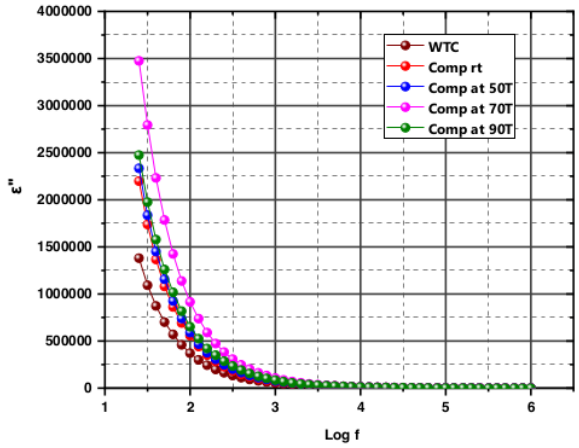

Fig. 4.8 : ε'' vs. $log\ F$ for TiO_2 based DSSC Prepared at different post deposition treatment (Hot Comp.) at (a) Without Comp. (b) Comp. at RT 40 MPa (c) Comp. at 50℃, 40 MPa (d) Comp. at 70℃, 40 MPa (e) Comp. at 90℃ at 40 MPa.

Fig. 4.7 and **Fig. 4.8** exhibits the logarithm value of frequency dependence of dielectric constant (ε') and dielectric loss (ε") respectively for the five different cells prepared at different compression condition namely (a) without comp. (b) Comp. at RT, 40MPa, (c) Comp. at 50T, 40MPa (d) comp. at 70T, 40MPa (e) comp. at 90T, 40MPa. The High dielectric constant (ε') and dielectric loss (ε'') over the low-frequency region are normally associate with to build-up of ions at the electrode/electrolyte interface of the samples doped with a concentration of TiO_2. As per observation, in Fig 4.9 when the frequency starts to increase, at the initial stage ε' increase until reach a highest peak of (ε') max and then decrease with the High frequency that is correlated to the reduction in polarization as a result of ions accumulation after rapid decrease of (ε') for High frequency this phenomenon can be either by an increase of the free carrier density which also leads to polarization decrease. from Fig. 4.10 (ε'') decreases while the measuring frequency increase. However for the High-frequency region for charge accumulation and decrease of interface polarization with increasing frequency and with less ionic diffusion in the field region both (ε') and (ε'') thus decrease after the log F cross the value from 3 to 6 in Fig. 4.9 and 4.10 [98].

4.4.5 M′ vs. log F, M" vs. log F

Using electrical modulus formalism, a more thorough investigation of dielectric performance might be accomplished. Modulus demonstration is useful for concealing the signal strength associated with electrode polarization [99]. Electric module curve provides to investigate conductivity relaxation phenomena for both ionic conductors and polymers [100]. Beside this electric module, formalism investigates and analysis the dielectric relaxation including electric transport mechanism such as carrier hopping rate, etc. The real and imaginary parts of complex electric modules (M*) using the following formula [99], [101].

$$M' = \frac{\varepsilon'}{\varepsilon'^2 + \varepsilon''^2} = \omega C_o z''$$

$$M'' = \frac{\varepsilon''}{\varepsilon'^2 + \varepsilon''^2} = \omega C_o z'$$

Where,

M' = Real part of electric Modulus .

M'' = Imaginary part of electric modulus.

Fig. 4.9 and **Fig. 4.10** show the M' vs. log f and M'' vs. log f respectively. In the lower frequency region M' shows moderately a minute value while a large value end at High frequency. In the low-frequency region for M' vs. log f electrode polarization value is absent. As the frequency increases the value of M' increase reaching M'(max) at High-frequency region. In Figure 4.12 a low value of M'' shows at low-frequency region which might be due to the great value of capacitance formation at the electrode [102]. For all actions, there is a steady increase in M'' with increasing frequency which leads to a constant values at High value of log frequency at different post deposition treatment mentioned in the Figure furthermore M'' reaches its highest value as a result of conduction phenomena [103].

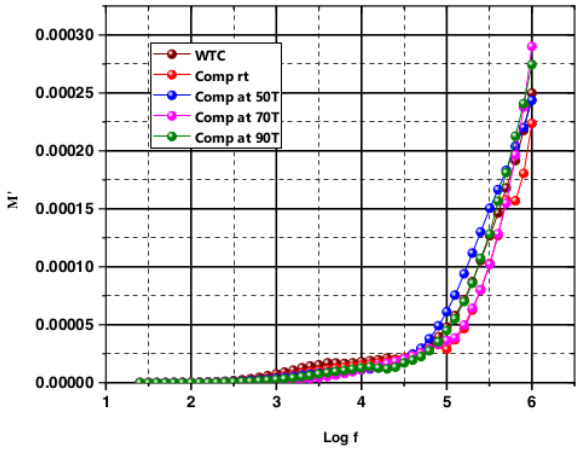

Fig. 4.9: M' vs. log f for TiO_2 based DSSC Prepared at different post deposition treatment (Hot Comp. at (a) Without Comp. (b) Comp. at RT, 40 MPa (c) Comp. at 50℃, 40 MPa (d) Comp. at 70℃, 40 MPa (e) Comp. at 90℃ at 40 MPa.

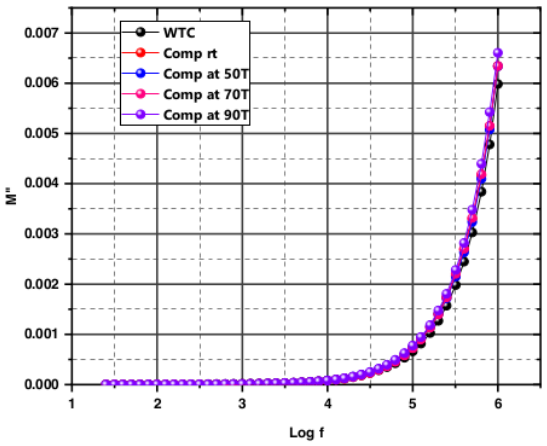

Fig. 4.10: M'' vs. $\log F$ for TiO_2 based DSSC Prepared at different post deposition treatment (Hot Comp.) at (a) Without Comp. (b) Comp. at RT, 40 MPa (c) Comp. at 50℃, 40 MPa (d) Comp. at 70℃, 40 MPa (e) Comp. at 90℃ at 40 MPa.

4.4.6 Dielectric loss tangent vs. log F

($\tan\delta$) is the ratio of imaginary permittivity (or dielectric loss) (ε'') to the real permittivity (or relative dielectric constant) (ε') which means

$$\text{Loss tangent} = \frac{\varepsilon''}{\varepsilon'} = tan\delta$$

Where 'δ' is the phase difference between the induced current in the material and applied $\tan\delta$ is taken as a measure of dielectric loss and is known as loss tangent. In short, $\tan\delta$ represent the loss amount for the dielectric constant in the above equation. $\tan\delta$ depended on the polarization of is space charge region, dielectric constant, porosity, vacancies, resistivity, capacitance, etc., of the devices and related to low and high frequencies. In **Fig. 4.11** shows the $\tan\delta$ vs. log F which can be used to provide information about the relaxation process. According to the principle of Koop's phenol nomological model $\tan\delta$ increase at a certain stage, until it reaches its maximum value with the increasing frequency and then it starts to decrease. With the increasing of $\tan\delta$ the ohmic component of the created current rises at a low-frequency region [98], [103]. At the High-frequency region, with the decreasing of $\tan\delta$

ohmic component is virtually frequency dependent [104]. In Figure 4.10 it is observed that the variation of the normalized loss tangent with frequency at different temperature regarding the post-deposition treatment of EIS, tan increase with the increase of frequency from the Figure 4.13 when the value of log F is increasing from value 2 to value 4, the tan value started to increase from its decrease position and at log f=6 we see the maximum rise of tan for all the five samples (Without Compression, Comp at RT, Comp at 50T, Comp at 70T, Comp at 90T) and if the frequency range is increased then there we may see the decreasing of tanδ. The frequency corresponding to the maximum value of tanδ would be shifted to the high value of tanδ would be shifted to the high-frequency side with different post-deposition temperature which is mentioned above. The lose of tangent peaks and move with temperature leads to a dielectric relaxation process [105].

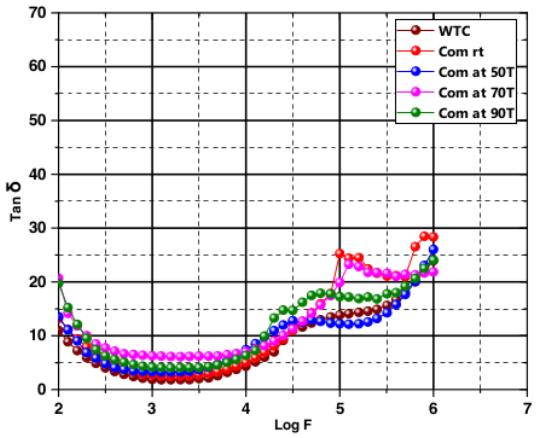

Fig. 4.11: Influence of Tanδ vs. $log\ f$ for TiO_2 based DSSC Prepared at different post deposition treatment (Hot Comp.) at (a) Without Comp. (b) Comp. at RT, 40 MPa (c) Comp. at 50℃, 40 MPa (d) Comp. at 70℃, 40 MPa (e) Comp. at 90℃ at 40 MPa.

4.4.7 Capacitance vs. log F for Impedance spectroscopy (EIS) analysis

The Impedance Spectroscopy technique is one of the popular and well-established methods for capacitance determination [106]. From the equation of determining Capacitance for impedance X, we get C=1/2πfx. which indicates an inverse relationship between Capacitance and frequency. The more the value of frequency increased the more the value of capacitance decreased significantly. From the graph, we see when the application of Log F is 1.39999 at

that point value of capacitance for WTO, comp at Rt, comp at 50T, comp at 70 T, and comp at 90 T are respectively 0.5886 F,0.96036 F,2.138 F, 2.098F and 2.113 F, which were highest at value when frequency at lower condition, but when the frequency was increasing from Log F= 2.5 up to at higher conditions which were found of 6, the value of capacitance at in (Without Compression, comp at RT, comp at 50 T, comp at 70T, comp at 90 T) was decreasing and at the end, found lowest and from the graph we observed that the values were so close to zero that we got a flat line of the curve at the result shown in **Fig 4.12**.

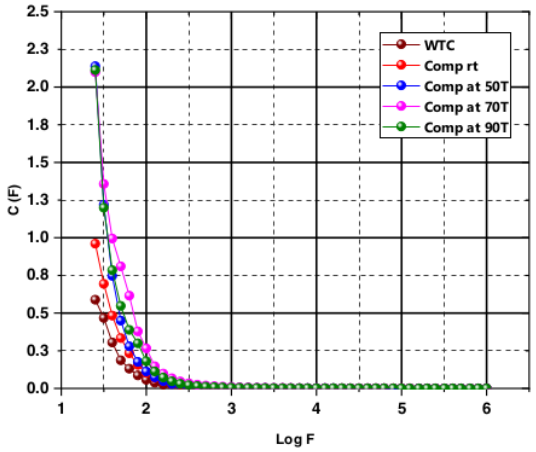

Fig. 4.12 : Capacitance vs. log F for TiO_2 based DSSC Prepared at different post deposition treatment (Hot Comp.) at (a) Without Comp. (b) Comp. at RT, 40 MPa (c) Comp. at 50℃, 40 MPa (d) Comp. at 70℃, 40 MPa (e) Comp. at 90℃ at 40 MPa.

4.5 I-V Characteristics

To understand the photovoltaic performance, the current density vs. voltage has showed in **Fig. 4.13** of the DSSC's varying different comp. temperature. Due to the enhancement of (τ) , V_{oc} is increased with the increasing of comp. temperature (RT to 70℃) from (0.713 – 0.714)V. The FF is found in stable condition. It is varying from 0.57 to 0.61 for different compression of (Without Compression, RT, 50T, 70T, 90T) and it was noticed that at room temperature compression it was found better than the rest. Photocurrent density, J_{sc} is increased from (RT to 90), J_{sc} value has seen about 6.88, 8.39, 9.30, and 7.92 mA/cm^2 respectively. Where for 70℃ the value of J_{sc} was worth mentioning. And finally, due to the

growth of photovoltaic parameter (V_{oc}, FF, J_{sc}), efficiency (η) is increased has been found 3.047 for RT, 3.366 for 50°C and **3.85** for 70°C comp. temperature **(maximum efficiency)**.

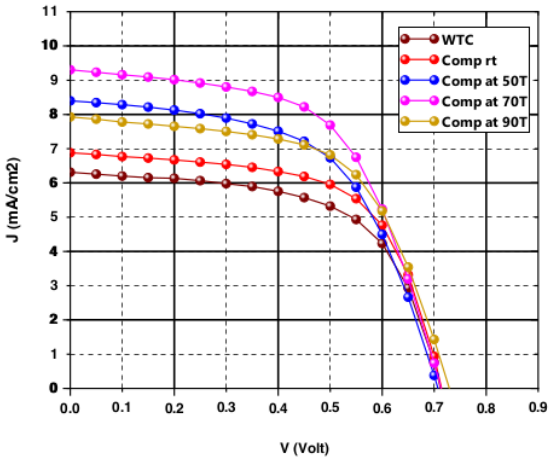

Fig. 4.13: Current density vs. Voltage plot for different comp. temperature (RT – 90°C) of DSSC.

Table 4.2 I-V Characteristics

	Thickness(μm)	J_{sc}(mA/cm^2)	V_{oc} (Volt)	FF	Eff (η) (%)
Without Comp.	14	6.32	0.712	0.603	2.714
Comp. at RT	12.5	6.88	0.714	0.62	3.047
Comp. at 50T	12.3	8.40	0.707	0.567	3.366
Comp. at 70T	12.1	9.30	0.714	0.579	3.85
Comp. at 90T	12.1	7.93	0.729	0.594	3.43

Value of I-V characteristics parameters are shown in **Table 4.2.**

Calculation Method of R_s and R_{sh} :

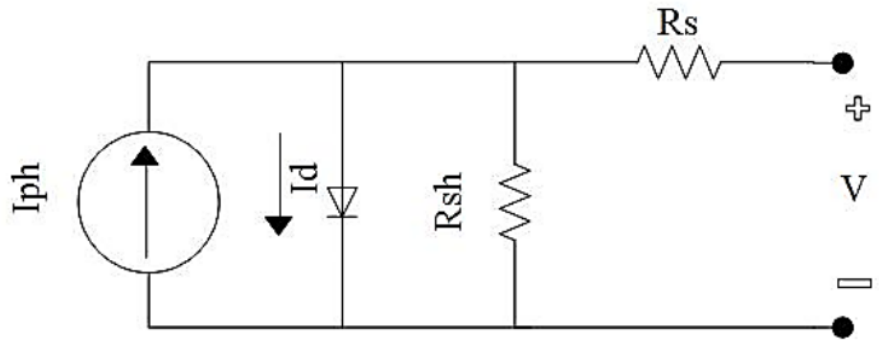

Fig. 4.14: Single diode circuit for I-V characteristic observation.

In **Fig. 4.14** is shown single diode circuit. At a certain level of lighting, the equation (1) from the Shockley equation gives the current/voltage relationship [107].

Now,

$$I = I_{ph} - I_o \left(e^{\frac{q(V+IR_s)}{V_T}} - 1\right) - \left(\frac{V+IR_s}{R_{sh}}\right) \quad \text{.....(1)}$$

Where, $V_T = \frac{N_s a k T}{q}$ .....(2)

I_{ph} = Photon current.

I_o = Reverse saturation current.

R_{sh} = Shunt resistance.

R_s = Series resistance.

a = Diode ideality factor.

V_{oc} = Open circuit voltage.

I_{sc} = Short circuit current.

N_s = No of cell in series.

$I_{ph} = I_{sc}$ = constant.

V_T = Thermal Voltage.

Estimation of R_{sh} (shunt resistance):

Now deriving of equation (1) we get,

$$\frac{dI}{dV} = -\frac{I_o}{V_T}\left(e^{\frac{V+IR_s}{V_T}}\left(1 + R_s\frac{dI}{dV}\right)\right) - \frac{1}{R_{sh}} - \frac{R_s}{R_{sh}}\frac{dI}{dV}$$

$$\frac{dI}{dV} = \left(1 + \frac{R_s}{R_{sh}} + \frac{I_o R_s}{V_T} e^{\frac{V+IR_s}{V_T}}\right) = -\frac{I_o}{V_T} e^{\frac{V+IR_s}{V_T}} - \frac{1}{R_{sh}} \dots\dots\dots\dots\dots\dots\dots\dots\dots\dots\dots (3)$$

Under short circuit condition

$$I_o e^{\frac{V+IR_s}{V_T}} = I_o e^{\frac{I_{sc}R_s}{V_T}} \approx 0 \quad \text{and} \quad R_s \ll R_{sh}$$

So from equation (3), we get,

$$\boxed{R_{sh} = -\frac{dV}{dI}\Big| \text{ (at short circuit)}}$$

Or inverse of the slope of the IV curve at short circuit.

Estimation of R_s (Series resistance):

R_s Significantly effect IV curve at open circuit condition,

From equation (3) we get,

$$\frac{dI}{dV}\left(1 + \frac{R_s}{R_{sh}} + \frac{I_o R_s}{R_{sh}} + \frac{I_o R_s}{V_T} e^{\frac{V+IR_s}{V_T}}\right) = -\frac{I_o}{V_T} e^{\frac{V+IR_s}{V_T}} - \frac{1}{R_{sh}}$$

Under open circuit condition:

$$I_o e^{\frac{V+IR_s}{V_T}} = I_o e^{\frac{V_{oc}}{V_T}} = I_{sc}$$

Hence from equation (3), we get,

$$\frac{dI}{dV}\left(1 + R_s\left(\frac{1}{R_{sh}} + \frac{I_{sc}}{V_T}\right)\right) = -\left(\frac{I_{sc}}{V_T} + \frac{1}{R_{sh}}\right)$$

or, $$\left(1 + R_s\left(\frac{1}{R_{sh}} + \frac{I_{sh}}{V_T}\right)\right) = -\frac{dV}{dI}\left(\frac{I_{sc}}{V_T} + \frac{1}{R_{sh}}\right)$$

so, $$R_s = -\frac{dV}{dI} - \frac{1}{\left(\frac{1}{R_{sh}} + \frac{I_{sh}}{V_T}\right)} \ldots\ldots\ldots\ldots\ldots\ldots\ldots (4)$$

with $$\frac{1}{R_{sh}} \ll \frac{I_{sc}}{V_T}$$

we get from equation (4) with $\frac{1}{R_{sh}} = 0$.

$$R_s = -\frac{dV}{dI}\Big|_{\text{at open}} - \frac{V_T}{I_{sc}}$$

Or inverse of slope in IV curve at open circuit condition.

Procedure of getting R_s, R_{sh} from I-V curve:

Shunt Resistance (R_{sh})

$$R_{sh} = -\frac{dV}{dI}\Big| \text{ at short circuit}$$

R_{sh} = Inverse of the slope of IV curve at short circuit

Require:

1. The angle of the I-V curve at the short circuit : θ_s.

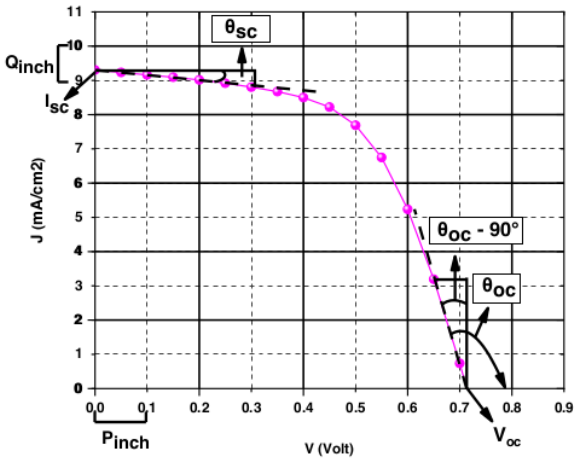

Fig. 4.15: Method of determining R_{sh} form I-V curve.

$$Y_{axis}\ \text{scale}: \frac{\text{the increasing rate of current}}{Q_{inch}}$$

$$X_{axis}\ \text{scale}: \frac{\text{the increasing rate of voltage}}{P_{inch}}$$

$$\left|\frac{dI}{dV}\right| \text{(at short circuit)}$$

$$= \tan(\theta_s) \times \frac{\text{the increasing rate of current}}{Q_{inch}} \times \frac{P_{inch}}{\text{the increasing rate of voltage}}$$

$$= \cdots A/v.$$

$$R_{sh} = -\left|\frac{dV}{dI}\right| (at\ short\ circuit) = \frac{-1}{\frac{dI}{dV}}$$

Series Resistance (R_s)

$$R_s = -\frac{dV}{dI} - \frac{V_T}{I_{sc}}$$

$R_s =$ inverse of the slope of the I-V curve at open circuit.

$$V_T = \frac{N_s aKT}{q}$$

Require:

2. The angle of I-V curve at open circuit = θ_{oc}.

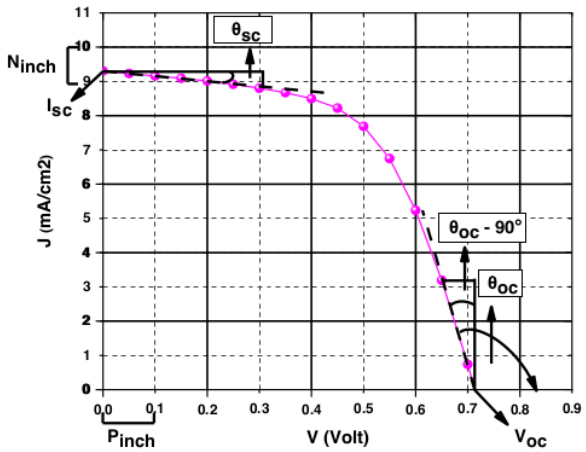

Fig. 4.16: Method of determining $\boldsymbol{R_s}$, form I-V curve.

$$\mathrm{Y_{axis}\ scale} = \frac{\text{the increasing rate of current}}{\mathrm{N_{inch}}}$$

$$\mathrm{X_{axis}\ scale} = \frac{\text{the increasing rate of voltage}}{\mathrm{M_{inch}}}$$

$$\left|\frac{\mathrm{dV}}{\mathrm{dI}}\right| \text{(at open circuit)}$$

$$= (-\tan(\theta oc - 90°)) \times \frac{\text{the increasing rate of voltage}}{M_{inch}} \times \frac{N_{inch}}{\text{the increasing rate of current}}$$

=..... V/A

$$\mathbf{R_s = -\frac{dV}{dI} - \frac{V_T}{I_{sc}}}$$

1. **With Out Compression :**

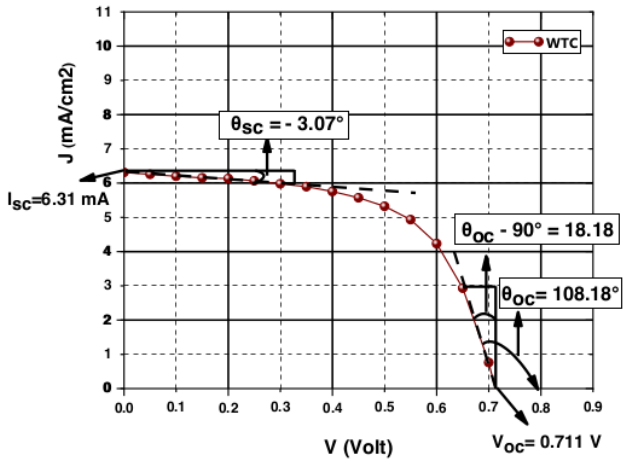

Fig. 4.17: R_s and R_{sh} determination by I-V curve (without compression)

From **Fig.4.17** of I-V,

$\theta_{oc} = 108.18°$

$\theta_{sc} = -3.07°$

$I_{sc} = 6.31\ mA$

$V_{oc} = 0.711\ V$

and, 1mA= 0.16 inch

0.1V=0.24 inch

Now,

$$\frac{dI}{dV}(\text{at short circuit}) = \tan(-3.07) \times \frac{1\times10^{-3}}{0.16} \times \frac{0.24}{0.1}$$

$$= -8.045 \times 10^{-4}\text{A/V}$$

$$R_{sh} = -\left.\frac{dV}{dI}\right| \text{at short circuit} = \frac{-1}{-8.04 \times 10^{-4}}$$

$$= \mathbf{1.243 \times 10^{3}\Omega}$$

$$R_s = -\frac{dV}{dI} - \frac{V_T}{I_{sc}}$$

$$\left.\frac{dV}{dI}\right| \text{at open circuit} = -\tan(108.18 - 90) \times \frac{0.1}{0.24} \times \frac{0.16}{1 \times 10^{-3}}$$

$$= -21.8 \ \frac{V}{A}$$

$$V_T = \frac{N_s aKT}{q} = \frac{1 \times 1 \times 1.38 \times 10^{-23} \times 273}{1.6 \times 10^{-19}}$$

$$= 0.0235 \text{ V}$$

$$R_s = -\frac{dV}{dI} - \frac{V_T}{I_{sc}}$$

$$= -(-21.8) - \frac{0.0235}{6.31 \times 10^{-3}}$$

$$\mathbf{R_s = 18.068\ \Omega}$$

2. **For Room Temperature:**

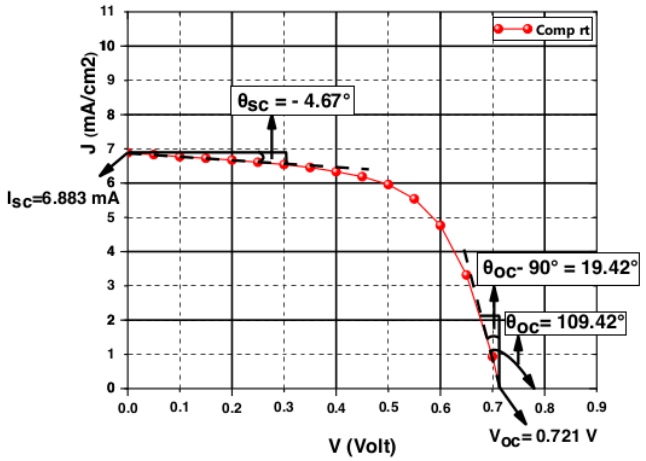

Fig. 4.18 : R_s and R_{sh} determination by I-V curve (compression at room temperature)**.**

From the **Fig. 4.18** of I-V

$\theta_{oc} = 109.42°$

$\theta_{sc} = -4.67°$

$I_{sc} = 6.883\ mA$

$V_{oc} = 0.721\ V$

and, 1mA= 0.16 inch

0.1V=0.24 inch

Now,

$$\left|\frac{dI}{dV}\right| \text{ at short circuit} = \tan(-4.67) \times \frac{1 \times 10^{-3}}{0.16} \times \frac{0.24}{0.1}$$

$$= -1.23 \times 10^{-3}\ \text{A/v}$$

$$R_{sh} = -\left|\frac{dV}{dI}\right| \text{ at short circuit} = \frac{-1}{-1.23 \times 10^{-3}}$$

$$= \mathbf{8.13 \times 10^{2}\Omega}$$

$$R_s = -\frac{dV}{dI} - \frac{V_T}{I_{sc}}$$

$$\left|\frac{dV}{dV}\right| \text{ at open circuit} = -\tan(109.42 - 90) \times \frac{0.1}{0.24} \times \frac{0.16}{1 \times 10^{-3}}$$

$$= -23.5\ \text{V/A}$$

$$V_T = \frac{N_s aKT}{q} = \frac{1 \times 1 \times 1.38 \times 10^{-23} \times 298}{1.6 \times 10^{-19}}$$

$$= 0.026\ \text{V}$$

$$R_s = -\frac{dV}{dI} - \frac{V_T}{I_{sc}}$$

$$= -(-23.5) - \frac{0.026}{6.883\times10^{-3}}$$

$$\boldsymbol{R_s = 19.72\ \Omega}$$

3. For 50 ℃ Compression :

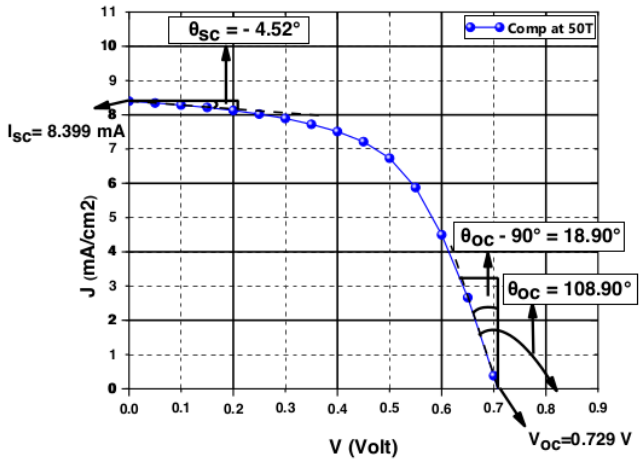

Fig. 4.19: R_s and R_{sh} determination by I-V curve (compression at 50°C)**.**

From the **Fig.4.19** of I-V,

$$\theta_{oc} = 108.90°$$
$$\theta_{sc} = -4.52°$$
$$I_{sc} = 8.399\ mA$$
$$V_{oc} = 0.729\ V$$

and, 1mA= 0.16 inch

0.1V=0.24 inch

Now,

$$\left|\frac{dI}{dV}\right| \text{ at short circuit} = \tan(-4.52) \times \frac{1\times10^{-3}}{0.16} \times \frac{0.24}{0.1}$$
$$= -1.185 \times 10^{-3}\ \text{A/v}$$

$$R_{sh} = -\left|\frac{dV}{dI}\right| \text{ at short circuit} = \frac{-1}{-1.185\times10^{-3}} = 8.43\times10^{2}\Omega$$

$$R_s = -\frac{dV}{dI} - \frac{V_T}{I_{sc}}$$

$$\left.\frac{dV}{dV}\right| \text{at open circuit} = -\tan(108.90 - 90) \times \frac{0.1}{0.24} \times \frac{0.16}{1 \times 10^{-3}}$$

$$= -22.83 \text{ V/A}$$

$$V_T = \frac{N_s aKT}{q} = \frac{1 \times 1 \times 1.38 \times 10^{-23} \times (273 + 50)}{1.6 \times 10^{-19}}$$

$$= 0.027 \text{ V}$$

$$R_s = -\frac{dV}{dI} - \frac{V_T}{I_{sc}}$$

$$= -(-22.83) - \frac{0.027}{8.39 \times 10^{-3}}$$

$$\boldsymbol{R_s = 19.61\ \Omega}$$

4. **For 70℃ Compression :**

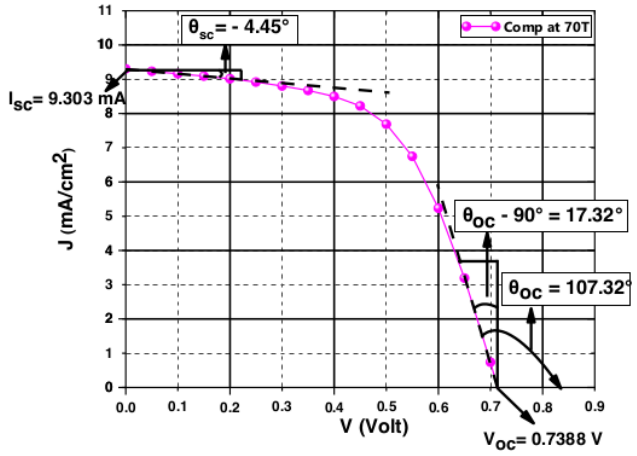

Fig. 4.20 : R_s and R_{sh} determination by I-V curve (compression at 70°C)**.**

From Fig.4.20 of **I-V,**

$$\theta_{oc} = 107.32°$$
$$\theta_{sc} = -4.45°$$
$$I_{sc} = 9.303\ mA$$
$$V_{oc} = 0.7388\ V$$

and, 1mA= 0.16 inch

0.1V=0.24 inch

Now,

$$\left.\frac{dI}{dV}\right| \text{at short circuit} = \tan(-4.45) \times \frac{1 \times 10^{-3}}{0.16} \times \frac{0.24}{0.1}$$
$$= -1.167 \times 10^{-3}\ \text{A/v}$$

$$R_{sh} = -\left.\frac{dV}{dI}\right| \text{at short circuit} = \frac{-1}{-1.167 \times 10^{-3}}$$
$$= \mathbf{8.57 \times 10^{2}\Omega}$$

$$R_s = -\frac{dV}{dI} - \frac{V_T}{I_{sc}}$$

$$\left.\frac{dV}{dV}\right| \text{at open circuit} = -\tan(107.32 - 90) \times \frac{0.1}{0.24} \times \frac{0.16}{1 \times 10^{-3}}$$
$$= -20.8\frac{V}{A}$$

$$V_T = \frac{N_s aKT}{q} = \frac{1 \times 1 \times 1.38 \times 10^{-23} \times (273 + 70)}{1.6 \times 10^{-19}}$$
$$= 0.029\ \text{V}$$

$$R_s = -\frac{dV}{dI} - \frac{V_T}{I_{sc}}$$

$$= -(-20.09) - \frac{0.029}{9.3 \times 10^{-3}}$$

$\mathbf{R_s = 17.6\ \Omega}$

5. **For 90℃ Compression :**

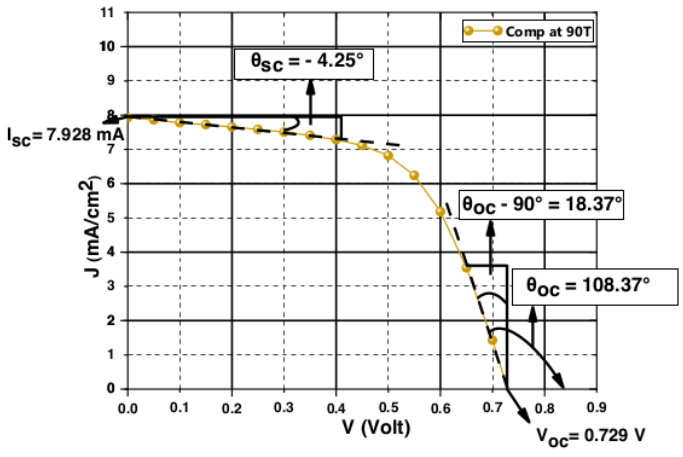

Fig. 4.21 : R_s and R_{sh} determination by I-V curve (compression at 90°C)**.**

From the Fig. 4.21 of I-V

$\theta_{oc} = 108.37°$

$\theta_{sc} = -4.25°$

$I_{sc} = 7.928\ mA$

$V_{oc} = 0.729\ V$

and, 1mA= 0.16 inch

0.1V=0.24 inch

Now,

$$\left|\frac{dI}{dV}\right| \text{ at short circuit} = \tan(-4.25) \times \frac{1\times10^{-3}}{0.16} \times \frac{0.24}{0.1}$$

$$= -1.11 \times 10^{-3}\ \text{A/V}$$

$$R_{sh} = -\left|\frac{dV}{dI}\right| \text{ at short circuit} = \frac{-1}{-1.11 \times 10^{-3}}$$

$= 9 \times 10^2 \Omega$

$$R_s = -\frac{dV}{dI} - \frac{V_T}{I_{sc}}$$

$$\left.\frac{dV}{dV}\right| \text{at open circuit} = -\tan(108.37 - 90) \times \frac{0.1}{0.24} \times \frac{0.16}{1 \times 10^{-3}}$$

$= -22.14\ V/A$

$$V_T = \frac{N_s aKT}{q} = \frac{1 \times 1 \times 1.38 \times 10^{-23} \times (273 + 90)}{1.6 \times 10^{-19}}$$

$$= 0.03$$

$$R_s = -\frac{dV}{dI} - \frac{V_T}{I_{sc}}$$

$$= -(-22.14) - \frac{0.03}{7.928 \times 10^{-3}}$$

$= 22.14 - 3.78$

$\mathbf{R_s = 18.35\ \Omega}$

So if we, summarize the I-V curve data we get the following **Table 4.3**,

Table 4.3 Parameters value of I-V curve at different post-treatment condition from the graph of the I-V curve we get

	θ_{oc}	$\theta_{oc} - 90$	θ_{sc}	$V_{oc}(V)$	J_{sc}(mA/cm^2)	R_s (Ω)	R_{sh}(Ω)
Without Compression	108.18°	18.18°	−3.07°	0.711	6.310	18.06	1.24×10^3
Compression at RT	109.42°	19.42°	−4.67°	0.721	6.883	19.72	8.13×10^2
Compression at 50 ℃	108.90°	18.90°	−4.52°	0.729	8.399	19.61	8.43×10^2
Compression at 70℃	107.32°	17.32°	−4.45°	0.739	9.303	17.6	8.57×10^2
Compression at 90℃	108.37°	18.37°	−4.25°	0.729	7.929	18.35	9×10^2

CHAPTER 5

CONCLUSION AND FUTURE WORK

5.1 Conclusion

To observe the effect of hot compression this investigation let us analyze data related to impedance characteristics through " Nyquist plot" or "Cole-Cole plot" data, Bode phase plot, real and imaginary part of impedance vs. Log F, Ɛ' and Ɛ " vs. Log Frequency, M' and M" vs. Log F, Capacitance (C) vs. Log Frequency, Loss $\tan\delta$ vs Log Frequency and the I-V curve characteristics of DSSC.

In the Nyquist plot, the decrease of charge transfer resistance (large semicircle at lower frequency) R_{ct} (AE), increases photovoltaic performance. The Bode phase plot shows the characteristic peak frequency (F_{max}) reduce for hot compression. The inverse relationship between electron life time (τ) and low-frequency peaks (F_{max}) shows the less the value of F_{max} the Higher the value of carrier lifetime of electron (τ). The proportional relation of open-circuit voltage (V_{oc}) and (τ) which is related to photovoltaic data shows good increment . To improve the layer quality after EPD techniques, The Hot compression makes the layer more compact which in turn improve the V_{oc} as well as efficiency of DSSC which is exactly illustrated in our analysis regarding impedance vs. Log F data analysis. The conductivity behavior of electrolytes is analyzed by Ɛ' and Ɛ'' vs. Log Frequency. The details I-V curve characteristic analysis gives the (Rs) and (Rsh) values calculated through I-V curve-based equation. The decreasing value of series resistance and increasing value of shunt resistance from the I-V curve improves the photovoltaic parameters value and so as the efficiency of the cell.

Thus this EIS analysis shows that with different hot compression temperature, the homogenous compact layer TiO_2 (P25) nanoparticle gives better conversion efficiency and improves the I-V curve characteristics performance which matches with the analysis of two resistances (Rs) and (Rsh) values determined from the slop of the I-V curve. The best result was identified for 40 MPa compressions at 70℃ with the efficiency of 3.85% with (V_{oc}) 0.7134 Volt, (Jsc) of 9.302 mA/cm^2, fill factor of 0.579. Thus this analysis of electron transport data shows that hot compression is an impactful post-deposition treatment that can be suitably applied in TiO_2 based DSSC applications.

5.2 Future work

The best conversion efficiency of 3.85% for 70℃ with optimum pressure of 40MPa is highlighted in this investigation. Though this efficiency result is not worthy of large scale production obtained for TiO_2 based DSSC still this efficiency may encourage the researchers

1) To use a new dye sensitizer to increase the efficiency and stability of DSSC for better photoelectric conversion efficiency

2) Develop counter electrode with better dye absorbance.

REFERENCES

[1] R. Williams, "Becquerel photovoltaic effect in binary compounds," *J. Chem. Phys.*, vol. 32, no. 5, pp. 1505–1514, 1960, doi: 10.1063/1.1730950.

[2] A. Omar, M. Syukri, and N. Abd, "Electron transport properties analysis of titanium dioxide dye-sensitized solar cells (TiO 2 -DSSCs) based natural dyes using electrochemical impedance spectroscopy concept : A review," *Sol. Energy*, vol. 207, no. April, pp. 1088–1121, 2020, doi: 10.1016/j.solener.2020.07.028.

[3] A. Geravand, S. Sharbati, and M. Danaie, "Optimize parameters of new fabricated n-CdTe/p-CdTe solar cell," *2017 25th Iran. Conf. Electr. Eng. ICEE 2017*, no. January 2018, pp. 412–416, 2017, doi: 10.1109/IranianCEE.2017.7985484.

[4] S. Lijima, "© 19 9 1 Nature Publishing Group 그라첼꺼," *Nature*, vol. 354, pp. 56–58, 1991.

[5] W. J. Jeong *et al.*, "Visible light-responsive titanium dioxide thin film prepared by reactive sputtering," *J. Nanosci. Nanotechnol.*, vol. 11, no. 2, pp. 1565–1568, 2011, doi: 10.1166/jnn.2011.3380.

[6] C. P. Lee, C. T. Li, and K. C. Ho, "Use of organic materials in dye-sensitized solar cells," *Mater. Today*, vol. 20, no. 5, pp. 267–283, 2017, doi: 10.1016/j.mattod.2017.01.012.

[7] U. Mehmood *et al.*, "Photovoltaic improvement and charge recombination reduction by aluminum oxide impregnated MWCNTs/TiO2 based photoanode for dye-sensitized solar cells," *Electrochim. Acta*, vol. 203, pp. 162–170, 2016, doi: 10.1016/j.electacta.2016.04.027.

[8] S. Iwata, S. ichiro Shibakawa, N. Imawaka, and K. Yoshino, "Stability of the current characteristics of dye-sensitized solar cells in the second quadrant of the current–voltage characteristics," *Energy Reports*, vol. 4, pp. 8–12, 2018, doi: 10.1016/j.egyr.2017.10.004.

[9] L. Song, P. Du, J. Xiong, F. Ko, and C. Cui, "Efficiency enhancement of dye-sensitized solar cells by optimization of electrospun ZnO nanowire/nanoparticle hybrid photoanode and combined modification," *Electrochim. Acta*, vol. 163, pp. 330–337, 2015, doi: 10.1016/j.electacta.2015.02.093.

[10] A. Hagfeldt, G. Boschloo, L. Sun, L. Kloo, and H. Pettersson, "Dye-Sensitized Solar Cells," pp. 6595–6663, 2010.

[11] D. Soni, P. Parsoya, B. K. Menariya, R. Vyas, and R. Ameta, "Photoelectrochemical cells," *Sol. Energy Convers. Storage Photochem. Modes*, vol. 414, no. November, pp. 29–53, 2015, doi: 10.1201/b19148.

[12] T. Zhang, W. Dong, M. Keeter-Brewer, S. Konar, R. N. Njabon, and Z. R. Tian, "Site-specific nucleation and growth kinetics in hierarchical nanosyntheses of branched ZnO crystallites," *J. Am. Chem. Soc.*, vol. 128, no. 33, pp. 10960–10968, 2006, doi: 10.1021/ja0631596.

[13] K. Kakiuchi, E. Hosono, and S. Fujihara, "Enhanced photoelectrochemical performance of ZnO electrodes sensitized with N-719," *J. Photochem. Photobiol. A Chem.*, vol. 179, no. 1–2, pp. 81–86, 2006, doi: 10.1016/j.jphotochem.2005.07.018.

[14] S. Chatterjee, I. B. Karki, D. S. Cells, T. Nanopowders, Z. O. Nanorods, and P. Properties, "Effect of Photoanodes on the Performance of Dye-Sensitized Solar," vol. 15, no. 3, pp. 62–68, 2019.

[15] A. E. Shalan, A. M. Elseman, and M. M. Rashad, "Controlling the Microstructure and Properties of Titanium Dioxide for Efficient Solar Cells," *Titan. Dioxide - Mater. a Sustain. Environ.*, 2018, doi: 10.5772/intechopen.72494.

[16] M. Quintana, T. Edvinsson, A. Hagfeldt, and G. Boschloo, "Comparison of dye-sensitized ZnO and TiO2 solar cells: Studies of charge transport and carrier lifetime," *J. Phys. Chem. C*, vol. 111, no. 2, pp. 1035–1041, 2007, doi: 10.1021/jp065948f.

[17] S. Zen, D. Saito, R. Ono, and T. Oda, "Low-temperature-sintered dye-sensitized solar cell using surface treatment of TiO2 photoelectrode with ultraviolet light," *Chem. Lett.*, vol. 42, no. 6, pp. 624–626, 2013,

doi: 10.1246/cl.130147.

[18] D. Zhang, T. Yoshida, and H. Minoura, "Low temperature synthesis of porous nanocrystalline TiO2 thick film for dye-sensitized solar cells by hydrothermal crystallization," *Chem. Lett.*, vol. 4, no. 9, pp. 874–875, 2002, doi: 10.1246/cl.2002.874.

[19] P. Trihutomo, S. Soeparman, D. Widhiyanuriyawan, and L. Yuliati, "Performance Improvement of Dye-Sensitized Solar Cell- (DSSC-) Based Natural Dyes by Clathrin Protein," *Int. J. Photoenergy*, vol. 2019, pp. 1–9, 2019, doi: 10.1155/2019/4384728.

[20] T. Miyasaka, M. Ikegami, and Y. Kijitori, "Photovoltaic Performance of Plastic Dye-Sensitized Electrodes Prepared by Low-Temperature Binder-Free Coating of Mesoscopic Titania," *J. Electrochem. Soc.*, vol. 154, no. 5, p. A455, 2007, doi: 10.1149/1.2712140.

[21] S. Datta, A. Dey, N. R. Singha, and S. Roy, "Enhanced performance of dye-sensitized solar cell with thermally stable natural dye-assisted TiO2/MnO2 bilayer-assembled photoanode," *Mater. Renew. Sustain. Energy*, vol. 9, no. 4, 2020, doi: 10.1007/s40243-020-00185-3.

[22] F. Kabir *et al*., "Improvement of efficiency of Dye Sensitized Solar Cells by optimizing the combination ratio of Natural Red and Yellow dyes," *Optik (Stuttg).*, vol. 179, no. October 2018, pp. 252–258, 2019, doi: 10.1016/j.ijleo.2018.10.150.

[23] L. Grinis, S. Dor, A. Ofir, and A. Zaban, "Electrophoretic deposition and compression of titania nanoparticle films for dye-sensitized solar cells," *J. Photochem. Photobiol. A Chem.*, vol. 198, no. 1, pp. 52–59, 2008, doi: 10.1016/j.jphotochem.2008.02.015.

[24] T. H. Meen, J. K. Tsai, Y. S. Tu, T. C. Wu, W. D. Hsu, and S. Chang, "Optimization of the dye-sensitized solar cell performance by mechanical compression," pp. 1–8, 2014.

[25] K. Ezaka, T. Yamamura, T. Yasufuku, N. Kishi, and T. Soga, "Low-temperature fabrication of dye-sensitized solar cells on plastic films by hot-pressing method," *Chem. Lett.*, vol. 42, no. 10, pp. 1263–1264, 2013, doi: 10.1246/cl.130582.

[26] M. S. H. Choudhury, N. Kishi, and T. Soga, "Effects of compression at elevated temperature for electrophorically deposited TiO2-based dye-sensitized solar cell," *Jpn. J. Appl. Phys.*, vol. 55, no. 1, 2016, doi: 10.7567/JJAP.55.01AE13.

[27] M. S. H. Choudhury, N. Kishi, and T. Soga, "Performance analysis of electrophorically deposited ZnO-based dye-sensitized solar cells prepared using compression at elevated temperature along with postannealing," *Jpn. J. Appl. Phys.*, vol. 55, no. 1, 2016, doi: 10.7567/JJAP.55.01AA16.

[28] M. S. H. Choudhury, N. Kishi, and T. Soga, "Compression of ZnO nanoparticle films at elevated temperature for flexible dye-sensitized solar cells," *J. Alloys Compd.*, vol. 656, pp. 476–480, 2016, doi: 10.1016/j.jallcom.2015.09.138.

[29] M. S. Haque Choudhury, N. Kishi, and T. Soga, "Hot-compress: A new postdeposition treatment for ZnO-based flexible dye-sensitized solar cells," *Mater. Res. Bull.*, vol. 80, pp. 135–138, 2016, doi: 10.1016/j.materresbull.2016.03.037.

[30] M. S. H. Choudhury, A. N. Sakib, M. Islam, A. A. Abuelwafa, M. Shafiul Alam, and T. Soga, "Influence of Compression and Hot-compression in Electron Transport in Dye-sensitized Solar Cells Studied by Electrochemical Impedance Spectroscopy Analysis," *2018 Int. Conf. Innov. Sci. Eng. Technol. ICISET 2018*, no. October, pp. 278–283, 2018, doi: 10.1109/ICISET.2018.8745600.

[31] S. N. Karthick, K. V. Hemalatha, S. K. Balasingam, F. Manik Clinton, S. Akshaya, and H. J. Kim, "Dye-sensitized solar cells: History, components, configuration, and working principle," *Interfacial Eng. Funct. Mater. Dye. Sol. Cells*, no. December, pp. 1–16, 2019, doi: 10.1002/9781119557401.ch1.

[32] Y. Xiao *et al*., "A dual function of high performance counter-electrode for stable quasi-solid-state dye-sensitized solar cells," *J. Power Sources*, vol. 241, pp. 373–378, 2013, doi: 10.1016/j.jpowsour.2013.04.091.

[33] M. A. Green, K. Emery, Y. Hishikawa, and W. Warta, “Solar cell efficiency tables (version 36),” no. June, pp. 346–352, 2010, doi: 10.1002/pip.1021.

[34] C. F. Cf, “MOLECULAR Electrochemical Photolysis of Water at a Semiconductor Electrode One and Two-dimensional Structure of Alpha-Helix and Beta-Sheet Forms of Poly (L-Alanine) shown by Specific Heat Measurements at Low Temperatures (1 . 5-20 K),” vol. 238, pp. 37–38, 1972.

[35] P. Wang, S. M. Zakeeruddin, J. E. Moser, M. K. Nazeeruddin, T. Sekiguchi, and M. Grätzel, “D © 2003,” vol. 2, no. June, 2003, doi: 10.1038/nmat904.

[36] Y. U. Bai, Y. Cao, J. Zhang, M. Wang, R. Li, and P. Wang, “High-performance dye-sensitized solar cells based on solvent-free electrolytes produced from eutectic melts,” vol. 7, no. August, 2008, doi: 10.1038/nmat2224.

[37] Y. C. Hiba, A. I. Slam, Y. W. Atanabe, R. K. Omiya, N. K. Oide, and L. H. A. N. Ã, “JJAP Express Letter Dye-Sensitized Solar Cells with Conversion Efficiency of 11 . 1 %,” vol. 45, no. 25, pp. 638–640, 2006, doi: 10.1143/JJAP.45.L638.

[38] V. A. G. Verjan, B. T. Navarrete, R. María, F. Navarro, J. N. D. De León, and J. M. R. Herrera, “Effect of - TiO 2 particle and pore size on DSSC efficiency,” *Mater. Renew. Sustain. Energy*, vol. 9, no. 2, pp. 1–8, 2020, doi: 10.1007/s40243-020-00173-7.

[39] A. Omar, M. Syukri, and N. Abd, “Electron transport properties analysis of titanium dioxide dye-sensitized solar cells (TiO 2 -DSSCs) based natural dyes using electrochemical impedance spectroscopy concept : A review,” *Sol. Energy*, vol. 207, no. July, pp. 1088–1121, 2020, doi: 10.1016/j.solener.2020.07.028.

[40] K. Sharma, V. Sharma, and S. S. Sharma, “Dye-Sensitized Solar Cells : Fundamentals and Current Status,” vol. 6, 2018.

[41] S. Ferrere, A. Zaban, and B. A. Gregg, “Dye Sensitization of Nanocrystalline Tin Oxide by Perylene Derivatives,” vol. 5647, no. 97, pp. 4490–4493, 1997.

[42] B. V Bergeron, A. Marton, G. Oskam, and G. J. Meyer, “Dye-Sensitized SnO 2 Electrodes with Iodide and Pseudohalide Redox Mediators,” vol. 2, pp. 937–943, 2005.

[43] J. Moser, S. M. Zakeeruddin, M. K. Nazeeruddin, and M. Gra, “Co II (dbbip) 22 + Complex Rivals Tri-iodide / Iodide Redox Mediator in Dye-Sensitized Photovoltaic Cells,” pp. 10461–10464, 2001.

[44] J. Wu, Z. Lan, S. Hao, P. Li, and J. Lin, “Progress on the electrolytes for dye-sensitized solar cells *,” no. May 2014, 2008, doi: 10.1351/pac200880112241.

[45] M. T. Ã, F. Ahlskog, and P. Lund, “Industrial sheet metals for nanocrystalline dye-sensitized solar cell structures,” vol. 90, pp. 2881–2893, 2006, doi: 10.1016/j.solmat.2006.05.002.

[46] H. A. Deepa, G. M. Madhu, and V. Venkatesham, “Performance evaluation of DSSC’s fabricated employing TiO2 and TiO2-ZnO nanocomposite as the photoanodes,” *Mater. Today Proc.*, no. xxxx, 2020, doi: 10.1016/j.matpr.2020.09.711.

[47] J. B. Baxter, A. M. Walker, K. Van Ommering, and E. S. Aydil, “Synthesis and characterization of ZnO nanowires and their integration into dye-sensitized solar cells,” *Nanotechnology*, vol. 17, no. 11, 2006, doi: 10.1088/0957-4484/17/11/S13.

[48] K. Park, Q. Zhang, B. B. Garcia, X. Zhou, Y. H. Jeong, and C. Cao, “Effect of an ultrathin TiO2 layer coated on submicrometer-sized ZnO nanocrystallite aggregates by atomic layer deposition on the performance of dye-sensitized solar cells,” *Adv. Mater.*, vol. 22, no. 21, pp. 2329–2332, 2010, doi: 10.1002/adma.200903219.

[49] M. Grätzel, “Dye-sensitized solar cells,” *J. Photochem. Photobiol. C Photochem. Rev.*, vol. 4, no. 2, pp. 145–153, 2003, doi: 10.1016/S1389-5567(03)00026-1.

[50] Q. Zhang, C. S. Dandeneau, X. Zhou, and C. Cao, “ZnO nanostructures for dye-sensitized solar cells,”

Adv. Mater., vol. 21, no. 41, pp. 4087–4108, 2009, doi: 10.1002/adma.200803827.

[51] J. J. Wu, G. R. Chen, C. C. Lu, W. T. Wu, and J. S. Chen, "Performance and electron transport properties of TiO2 nanocomposite dye-sensitized solar cells," *Nanotechnology*, vol. 19, no. 10, 2008, doi: 10.1088/0957-4484/19/10/105702.

[52] L. Zhu *et al.*, "Performances of znO-based dye sensitized solar cells fabricated by hydrothermal synthesis and sol-gel technique," *Chinese Phys. Lett.*, vol. 26, no. 1, 2009, doi: 10.1088/0256-307X/26/1/018401.

[53] H. Yu, S. Zhang, H. Zhao, G. Will, and P. Liu, "An efficient and low-cost TiO2 compact layer for performance improvement of dye-sensitized solar cells," *Electrochim. Acta*, vol. 54, no. 4, pp. 1319–1324, 2009, doi: 10.1016/j.electacta.2008.09.025.

[54] P. Gnida *et al.*, "Impact of TiO2 nanostructures on dye-sensitized solar cells performance," *Materials (Basel).*, vol. 14, no. 7, pp. 13–15, 2021, doi: 10.3390/ma14071633.

[55] T. Covered and C. Properties, "Titanium Dioxide (TiO2) emiconductor ," pp. 2–5, 2013.

[56] X. Diffraction, *Standard X-ray Diffraction Powder Patterns*, no. 18. 1981.

[57] A. Bally, "ELECTRONIC PROPERTIES OF NANO-CRYSTALLINE TITANIUM DIOXIDE THIN FILMS," vol. 2094, 1999.

[58] "Physica 1," vol. 192, pp. 233–237, 1993.

[59] D. A. H. Hanaor and C. C. Sorrell, "Review of the anatase to rutile phase transformation," pp. 855–874, 2011, doi: 10.1007/s10853-010-5113-0.

[60] P. Yousef *et al.*, "Visible Light Responsive Titanium Dioxide (TiO 2)," vol. 19, no. 1, pp. 1–16, 2008.

[61] I. O. P. C. Series and M. Science, "Characterization of TiO 2 nanopaint for automotive application," 2020, doi: 10.1088/1757-899X/863/1/012053.

[62] A. Phys and S. Uchida, "Optimization of TiO2 compact layer formed by atomic layer deposition for efficient perovskite solar cells Optimization of TiO 2 compact layer formed by atomic layer deposition for efficient perovskite solar cells," vol. 203902, no. November, 2019, doi: 10.1063/1.5120307.

[63] A. E. S. M. R. M. M. Rashad, "Organic acid precursor synthesis and environmental photocatalysis applications of mesoporous anatase TiO 2 doped with different transition metal ions," pp. 3141–3146, 2014, doi: 10.1007/s10854-014-1995-y.

[64] A. E. Shalan, A. E. Shalan, A. M. Elseman, and A. M. Elseman, "Controlling the Microstructure and Properties of Controlling the Microstructure and Properties of Titanium Dioxide for Efficient Solar Cells Titanium Dioxide for Efficient Solar Cells," doi: 10.5772/intechopen.72494.

[65] V. Madurai, S. Pitchaiya, A. Pugazhendhi, and D. Velauthapillai, "ScienceDirect Performance of TiO 2 nanoparticles synthesized by microwave and solvothermal methods as photoanode in dye-sensitized solar cells (DSSC)," *Int. J. Hydrogen Energy*, no. xxxx, 2020, doi: 10.1016/j.ijhydene.2020.07.018.

[66] K. Tennakone, G. R. R. A. Kumara, I. R. M. Kottegoda, and V. P. S. Perera, "An efficient dye-sensitized photoelectrochemical solar cell made from oxides of tin and zinc," no. November 1998, pp. 15–16, 1999.

[67] K. Nazeeruddin, E. Baranoff, and M. Gra, "Dye-sensitized solar cells : A brief overview," vol. 85, pp. 1172–1178, 2011, doi: 10.1016/j.solener.2011.01.018.

[68] P. Trihutomo, S. Soeparman, D. Widhiyanuriyawan, and L. Yuliati, "Performance Improvement of Dye-Sensitized Solar Cell- (DSSC-) Based Research Article Performance Improvement of Dye-Sensitized Solar Cell- (DSSC-) Based Natural Dyes by Clathrin Protein," no. February, 2020.

[69] J. Gong, K. Sumathy, Q. Qiao, and Z. Zhou, "crossmark," *Renew. Sustain. Energy Rev.*, vol. 68, no. December 2015, pp. 234–246, 2017, doi: 10.1016/j.rser.2016.09.097.

[70] J. B. Baxter and J. B. Baxter, “needs to improve efficiency , stability , and manufacturing Commercialization of dye sensitized solar cells : Present status and future research needs to improve efficiency , stability , and manufacturing,” vol. 020801, no. May, 2014, doi: 10.1116/1.3676433.

[71] K. Patil, S. Rashidi, H. Wang, and W. Wei, “Review Article Recent Progress of Graphene-Based Photoelectrode Materials for Dye-Sensitized Solar Cells,” vol. 2019, 2019.

[72] L. Besra and M. Liu, “A review on fundamentals and applications of electrophoretic deposition (EPD),” *Prog. Mater. Sci.*, vol. 52, no. 1, pp. 1–61, 2007, doi: 10.1016/j.pmatsci.2006.07.001.

[73] J. G. P. Binner, “ADVANCED CERAMIC PROCESSING AND.”

[74] N. M. Structures, “Handbook of Nanoelectrochemistry,” *Handb. Nanoelectrochemistry*, no. June, 2016, doi: 10.1007/978-3-319-15207-3.

[75] M. S. H. Choudhury, S. R. Ahmed, M. Munirul Islam Tusher, M. A. Uddin, M. Shafiul Alam, and T. Soga, “Optimization of Electrophoretic Deposition Parameters for Uniform Titanium Oxide Deposition on Conductive Glass Substrate,” *2018 Int. Conf. Innov. Sci. Eng. Technol. ICISET 2018*, no. October, pp. 294–298, 2018, doi: 10.1109/ICISET.2018.8745573.

[76] G. Kim, H. Seo, V. P. Godble, Y. Kim, O. Yang, and H. Shin, “Electrophoretic deposition of titanate nanotubes from commercial titania nanoparticles : Application to dye-sensitized solar cells,” vol. 8, pp. 961–966, 2006, doi: 10.1016/j.elecom.2006.03.037.

[77] L. Shooshtari, M. Rahman, F. Tajabadi, and N. Taghavinia, “TiO 2 Fibers Enhance Film Integrity and Photovoltaic Performance for Electrophoretically Deposited Dye Solar Cell Photoanodes,” pp. 638–641, 2011.

[78] J. Yum, S. Kim, D. Kim, and Y. Sung, “Electrophoretically deposited TiO 2 photo-electrodes for use in flexible dye-sensitized solar cells,” vol. 173, pp. 1–6, 2005, doi: 10.1016/j.jphotochem.2004.12.023.

[79] T. Miyasaka, Y. Kijitori, J. E. Soc, P. A-a, and T. Layers, “Low-Temperature Fabrication of Dye-Sensitized Plastic Electrodes by Electrophoretic Preparation of Mesoporous TiO 2 Layers service Low-Temperature Fabrication of Dye-Sensitized Plastic Electrodes by Electrophoretic Preparation of Mesoporous,” vol. 151, no. 11, 2004, doi: 10.1149/1.1796931.

[80] J. Bandy, Q. Zhang, and G. Cao, “Electrophoretic Deposition of Titanium Oxide Nanoparticle Films for Dye-Sensitized Solar Cell Applications,” *Mater. Sci. Appl.*, vol. 02, no. 10, pp. 1427–1431, 2011, doi: 10.4236/msa.2011.210193.

[81] H. Chen *et al.*, “Electrochimica Acta Electrophoretic deposition of TiO 2 film on titanium foil for a flexible dye-sensitized solar cell &,” *Electrochim. Acta*, vol. 56, no. 23, pp. 7991–7998, 2011, doi: 10.1016/j.electacta.2010.10.099.

[82] “© 19 9 1 Nature Publishing Group.”

[83] M. S. H. Choudhury, N. Kishi, and T. Soga, “Hot-compression: An effective postdeposition treatment for electrophoretically deposited dye-sensitized solar cell,” *2017 IEEE 44th Photovolt. Spec. Conf. PVSC 2017*, pp. 3323–3326, 2017, doi: 10.1109/PVSC.2017.8366351.

[84] D. Sengupta, P. Das, B. Mondal, and K. Mukherjee, “Effects of doping , morphology and film-thickness of photo-anode materials for dye sensitized solar cell application – A review Effects of doping , morphology and fi lm-thickness of photo-anode materials for dye sensitized solar cell application – A revie,” *Renew. Sustain. Energy Rev.*, vol. 60, no. July, pp. 356–376, 2016, doi: 10.1016/j.rser.2016.01.104.

[85] M. S. H. Choudhury, A. N. Sakib, M. Islam, A. A. Abuelwafa, M. Shafiul Alam, and T. Soga, “Influence of Compression and Hot-compression in Electron Transport in Dye-sensitized Solar Cells Studied by Electrochemical Impedance Spectroscopy Analysis,” *2018 Int. Conf. Innov. Sci. Eng. Technol.*, no. October, pp. 278–283, 2019, doi: 10.1109/iciset.2018.8745600.

[86] A. Lasia, *Electrochemical Impedance Spectroscopy and its. .*

[87] E. J. Olson and P. Buhlmann, “Minimizing Hazardous Waste in the Undergraduate Analytical Laboratory: A Microcell for Electrochemistry,” vol. 87, no. 11, pp. 10–11, 2010.

[88] R. Kern, R. Sastrawan, J. Ferber, R. Stangl, and J. Luther, “Modeling and interpretation of electrical impedance spectra of dye solar cells operated under open-circuit conditions,” vol. 47, pp. 4213–4225, 2002.

[89] *Theory , Experiment , and* . .

[90] D. L. Losee and D. L. Losee, “Admittance spectroscopy of impurity levels in Schottky barriers Admittance spectroscopy of impurity levels in Schottky barriers,” vol. 2204, 1975, doi: 10.1063/1.321865.

[91] S. Sarker, A. J. S. Ahammad, H. W. Seo, and D. M. Kim, “Electrochemical impedance spectra of dye-sensitized solar cells: Fundamentals and spreadsheet calculation,” *Int. J. Photoenergy*, vol. 2014, no. November, 2014, doi: 10.1155/2014/851705.

[92] Q. Wang, J. Moser, and M. Gra, “Electrochemical Impedance Spectroscopic Analysis of Dye-Sensitized Solar Cells,” pp. 14945–14953, 2005.

[93] J. H. Yum *et al*., “Phosphorescent energy relay dye for improved light harvesting response in liquid dye-sensitized solar cells,” *Energy Environ. Sci.*, vol. 3, no. 4, pp. 434–437, 2010, doi: 10.1039/b925473k.

[94] S. Ito *et al*., “High-efficiency (7.2%) flexible dye-sensitized solar cells with Ti-metal substrate for nanocrystalline-TiO2 photoanode,” *Chem. Commun.*, no. 38, pp. 4004–4006, 2006, doi: 10.1039/b608279c.

[95] H. Rahmouni, M. Smari, B. Cherif, E. Dhahri, and K. Khirouni, “Conduction mechanism, impedance spectroscopic investigation and dielectric behavior of La0.5Ca0.5-xAgxMnO3 manganites with compositions below the concentration limit of silver solubility in perovskites ($0 \leq x \leq 0.2$),” *Dalt. Trans.*, vol. 44, no. 22, pp. 10457–10466, 2015, doi: 10.1039/c5dt00444f.

[96] P. Khatri, B. Behera, V. Srinivas, and R. N. P. Choudhary, “Complex impedance spectroscopic properties of Ba3V 2O8 ceramics,” *Adv. Mater. Sci. Eng.*, vol. 2008, pp. 1–6, 2008, doi: 10.1155/2008/746256.

[97] M. Okutan and E. Şentürk, “β Dielectric relaxation mode in side-chain liquid crystalline polymer film,” *J. Non. Cryst. Solids*, vol. 354, no. 14, pp. 1526–1530, 2008, doi: 10.1016/j.jnoncrysol.2007.08.085.

[98] S. B. Aziz and S. M. Mamand, “The Study of dielectric properties and conductivity relaxation of ion conducting chitosan: NaTf based solid electrolyte,” *Int. J. Electrochem. Sci.*, vol. 13, no. 11, pp. 10274–10288, 2018, doi: 10.20964/2018.11.05.

[99] S. B. Aziz, “Role of dielectric constant on ion transport: Reformulated Arrhenius equation,” *Adv. Mater. Sci. Eng.*, vol. 2016, 2016, doi: 10.1155/2016/2527013.

[100] S. B. Aziz, Z. H. Z. Abidin, and A. K. Arof, “Influence of silver ion reduction on electrical modulus parameters of solid polymer electrolyte based on chitosansilver triflate electrolyte membrane,” *Express Polym. Lett.*, vol. 4, no. 5, pp. 300–310, 2010, doi: 10.3144/expresspolymlett.2010.38.

[101] S. B. Aziz, “The Mixed Contribution of Ionic and Electronic Carriers to Conductivity in Chitosan Based Solid Electrolytes Mediated by CuNt Salt,” *J. Inorg. Organomet. Polym. Mater.*, vol. 28, no. 5, pp. 1942–1952, 2018, doi: 10.1007/s10904-018-0862-3.

[102] S. B. Aziz, M. A. Rasheed, and Z. H. Z. Abidin, “Optical and Electrical Characteristics of Silver Ion Conducting Nanocomposite Solid Polymer Electrolytes Based on Chitosan,” *J. Electron. Mater.*, vol. 46, no. 10, pp. 6119–6130, 2017, doi: 10.1007/s11664-017-5515-8.

[103] S. B. Aziz, R. B. Marif, M. A. Brza, M. H. Hamsan, and M. F. Z. Kadir, “Employing of Trukhan model to estimate ion transport parameters in PVA based solid polymer electrolyte,” *Polymers (Basel).*, vol. 11, no. 10, 2019, doi: 10.3390/polym11101694.

[104] S. B. Aziz, A. S. Marf, E. M. A. Dannoun, M. A. Brza, and R. M. Abdullah, "The study of the degree of crystallinity, electrical equivalent circuit, and dielectric properties of polyvinyl alcohol (PVA)-based biopolymer electrolytes," *Polymers (Basel).*, vol. 12, no. 10, pp. 1–17, 2020, doi: 10.3390/polym12102184.

[105] N. S. Wadatkar and S. A. Waghuley, "Studies on properties of as-synthesized conducting polythiophene through aqueous chemical route," *J. Mater. Sci. Mater. Electron.*, vol. 27, no. 10, pp. 10573–10581, 2016, doi: 10.1007/s10854-016-5152-7.

[106] O. Almora, C. Aranda, E. Mas-Marzá, and G. Garcia-Belmonte, "On Mott-Schottky analysis interpretation of capacitance measurements in organometal perovskite solar cells," *Appl. Phys. Lett.*, vol. 109, no. 17, 2016, doi: 10.1063/1.4966127.

[107] M. Diantoro, T. Suprayogi, A. Hidayat, A. Taufiq, A. Fuad, and R. Suryana, "Shockley ' s Equation Fit Analyses for Solar Cell Parameters from I-V Curves," vol. 2018, 2018.

ET163005 & ET163007_DSHC_(EIS analysis to find the effect of compression temp on P25 based DSSC)_Final report

ORIGINALITY REPORT

20%	13%	9%	7%
SIMILARITY INDEX	INTERNET SOURCES	PUBLICATIONS	STUDENT PAPERS

PRIMARY SOURCES

1	dspace.iiuc.ac.bd Internet Source	1%
2	nitech.repo.nii.ac.jp Internet Source	1%
3	Submitted to University of Wales Swansea Student Paper	1%
4	tel.archives-ouvertes.fr Internet Source	<1%
5	Submitted to Kenyatta University Student Paper	<1%
6	Lai, Fang-I, Jui-Fu Yang, and Shou-Yi Kuo. "Efficiency Enhancement of Dye-Sensitized Solar Cells' Performance with ZnO Nanorods Grown by Low-Temperature Hydrothermal Reaction", Materials, 2015. Publication	<1%
7	avs.scitation.org Internet Source	<1%

8	nanoscalereslett.springeropen.com Internet Source	<1 %
9	mafiadoc.com Internet Source	<1 %
10	Azimah Omar, Mohd Syukri Ali, Nasrudin Abd Rahim. "Electron transport properties analysis of titanium dioxide dye-sensitized solar cells (TiO2-DSSCs) based natural dyes using electrochemical impedance spectroscopy concept: A review", Solar Energy, 2020 Publication	<1 %
11	"Interfacial Engineering in Functional Materials for Dye - Sensitized Solar Cells", Wiley, 2019 Publication	<1 %
12	Submitted to Savitribai Phule Pune University Student Paper	<1 %
13	www.gamry.com Internet Source	<1 %
14	www.energysage.com Internet Source	<1 %
15	Submitted to University of Leeds Student Paper	<1 %
16	www.mdpi.com Internet Source	<1 %

17	H.A. Deepa, G.M. Madhu, V. Venkatesham. "Performance evaluation of DSSC's fabricated employing TiO2 and TiO2-ZnO nanocomposite as the photoanodes", Materials Today: Proceedings, 2020 Publication	<1 %
18	Alexandria R. C. Bredar, Amanda L. Chown, Andricus R. Burton, Byron H. Farnum. "Electrochemical Impedance Spectroscopy of Metal Oxide Electrodes for Energy Applications", ACS Applied Energy Materials, 2020 Publication	<1 %
19	dokumen.pub Internet Source	<1 %
20	www.readbag.com Internet Source	<1 %
21	shizuoka.repo.nii.ac.jp Internet Source	<1 %
22	H. Rahmouni, M. Smari, B. Cherif, E. Dhahri, K. Khirouni. " Conduction mechanism, impedance spectroscopic investigation and dielectric behavior of La Ca Ag MnO manganites with compositions below the concentration limit of silver solubility in perovskites (0 ≤ x ≤ 0.2) ", Dalton Transactions, 2015	<1 %

Publication

23	Sengupta, D., P. Das, B. Mondal, and K. Mukherjee. "Effects of doping, morphology and film-thickness of photo-anode materials for dye sensitized solar cell application – A review", Renewable and Sustainable Energy Reviews, 2016. Publication	<1 %
24	Submitted to Ibrahim Babangida University Student Paper	<1 %
25	Anders Hagfeldt, Gerrit Boschloo, Licheng Sun, Lars Kloo, Henrik Pettersson. "Dye-Sensitized Solar Cells", Chemical Reviews, 2010 Publication	<1 %
26	Submitted to University of Nairobi Student Paper	<1 %
27	erepository.uonbi.ac.ke Internet Source	<1 %
28	Lee, K.-M.. "Incorporating carbon nanotube in a low-temperature fabrication process for dye-sensitized TiO"2 solar cells", Solar Energy Materials and Solar Cells, 200812 Publication	<1 %
29	Submitted to Yeungnam University Student Paper	<1 %

30	Md. Shamimimul Haque Choudhury, Naoki Kishi, Tetsuo Soga. "Hot-compression: An effective postdeposition treatment for electrophoretically deposited dye-sensitized solar cell", 2017 IEEE 44th Photovoltaic Specialist Conference (PVSC), 2017 Publication	<1 %
31	Qing Wang, Jacques-E. Moser, Michael Grätzel. "Electrochemical Impedance Spectroscopic Analysis of Dye-Sensitized Solar Cells", The Journal of Physical Chemistry B, 2005 Publication	<1 %
32	Submitted to CSU, San Jose State University Student Paper	<1 %
33	cwww.intechopen.com Internet Source	<1 %
34	Choudhury, Md. Shamimul Haque, Naoki Kishi, and Tetsuo Soga. "Effects of compression at elevated temperature for electrophorically deposited TiO2-based dye-sensitized solar cell", Japanese Journal of Applied Physics, 2016. Publication	<1 %
35	Submitted to International Islamic University Chittagong Student Paper	<1 %

36	digilib.library.usp.ac.fj Internet Source	<1 %
37	link.springer.com Internet Source	<1 %
38	M. S. H. Choudhury, An Nazmus Sakib, Mobinul Islam, A. A. Abuelwafa, M. Shafiul Alam, T. Soga. "Influence of Compression and Hot-compression in Electron Transport in Dye-sensitized Solar Cells Studied by Electrochemical Impedance Spectroscopy Analysis", 2018 International Conference on Innovations in Science, Engineering and Technology (ICISET), 2018 Publication	<1 %
39	www.science.gov Internet Source	<1 %
40	doras.dcu.ie Internet Source	<1 %
41	pt.scribd.com Internet Source	<1 %
42	www.tandfonline.com Internet Source	<1 %
43	Submitted to Nexford University Student Paper	<1 %
44	www.hindawi.com Internet Source	<1 %

45	Subrata Sarker, A. J. Saleh Ahammad, Hyun Woo Seo, Dong Min Kim. "Electrochemical Impedance Spectra of Dye-Sensitized Solar Cells: Fundamentals and Spreadsheet Calculation", International Journal of Photoenergy, 2014 Publication	<1 %
46	Submitted to University of Southampton Student Paper	<1 %
47	mro.massey.ac.nz Internet Source	<1 %
48	res.mdpi.com Internet Source	<1 %
49	Submitted to Ho Chi Minh University of Technology and Education Student Paper	<1 %
50	Submitted to Universiti Sains Malaysia Student Paper	<1 %
51	Submitted to University of Essex Student Paper	<1 %
52	Submitted to Universiti Tenaga Nasional Student Paper	<1 %
53	etheses.whiterose.ac.uk Internet Source	<1 %
54	www.intechopen.com	

	Internet Source	<1%
55	Submitted to PSB Academy (ACP eSolutions) Student Paper	<1%
56	hdl.handle.net Internet Source	<1%
57	www.ncbi.nlm.nih.gov Internet Source	<1%
58	Norasikin A. Ludin, A.M. Al-Alwani Mahmoud, Abu Bakar Mohamad, Abd. Amir H. Kadhum et al. "Review on the development of natural dye photosensitizer for dye-sensitized solar cells", Renewable and Sustainable Energy Reviews, 2014 Publication	<1%
59	Submitted to Universiti Teknologi MARA Student Paper	<1%
60	etd.lib.metu.edu.tr Internet Source	<1%
61	pubs.rsc.org Internet Source	<1%
62	researchspace.auckland.ac.nz Internet Source	<1%
63	Submitted to Amity University Student Paper	<1%

64	Suman Chatterjee, Indra Bahadur Karki. "Effect of Photoanodes on the Performance of Dye-Sensitized Solar Cells", Journal of the Institute of Engineering, 2020 Publication	<1 %
65	repository.bilkent.edu.tr Internet Source	<1 %
66	Submitted to Universiti Brunei Darussalam Student Paper	<1 %
67	Submitted to Visvesvaraya Technological University Student Paper	<1 %
68	vdocuments.site Internet Source	<1 %
69	Submitted to University College London Student Paper	<1 %
70	Submitted to Nottingham Trent University Student Paper	<1 %
71	"Encyclopedia of Applied Electrochemistry", Springer Nature, 2014 Publication	<1 %
72	Submitted to Cranfield University Student Paper	<1 %
73	Koide, N.. "Improvement of efficiency of dye-sensitized solar cells based on analysis of	<1 %

equivalent circuit", Journal of Photochemistry & Photobiology, A: Chemistry, 20060910
Publication

74	Thin Film Structures in Energy Applications, 2015. Publication	<1 %
75	Submitted to Universiti Teknologi Malaysia Student Paper	<1 %
76	eprints-phd.biblio.unitn.it Internet Source	<1 %
77	porto.polito.it Internet Source	<1 %
78	Submitted to University of Pretoria Student Paper	<1 %
79	Submitted to Institute of Graduate Studies, UiTM Student Paper	<1 %
80	Submitted to Politecnico di Milano Student Paper	<1 %
81	baadalsg.inflibnet.ac.in Internet Source	<1 %
82	en.wikipedia.org Internet Source	<1 %
83	mts.intechopen.com Internet Source	<1 %

84	scholarcommons.usf.edu Internet Source	<1%
85	Gratzel, M.. "Conversion of sunlight to electric power by nanocrystalline dye-sensitized solar cells", Journal of Photochemistry & Photobiology, A: Chemistry, 20040601 Publication	<1%
86	Qifeng Zhang. "ZnO Nanostructures for Dye-Sensitized Solar Cells", Advanced Materials, 07/06/2009 Publication	<1%
87	Submitted to Xiamen University Student Paper	<1%
88	Jason B. Baxter. "Commercialization of dye sensitized solar cells: Present status and future research needs to improve efficiency, stability, and manufacturing", Journal of Vacuum Science & Technology A: Vacuum, Surfaces, and Films, 2012 Publication	<1%
89	Submitted to SASTRA University Student Paper	<1%
90	Submitted to Universiti Malaysia Perlis Student Paper	<1%
91	aip.scitation.org Internet Source	<1%

92	scholarbank.nus.edu.sg Internet Source	<1 %
93	Submitted to Oklahoma State University - Oklahoma City Student Paper	<1 %
94	Shujahadeen B. Aziz, Ayub S. S. Marf, Elham M. A. Dannoun, Mohamad A. Brza, Ranjdar M. Abdullah. "The Study of the Degree of Crystallinity, Electrical Equivalent Circuit, and Dielectric Properties of Polyvinyl Alcohol (PVA)-Based Biopolymer Electrolytes", Polymers, 2020 Publication	<1 %
95	Submitted to University of Nottingham Student Paper	<1 %
96	Xiaobo Chen, Samuel S. Mao. "Titanium Dioxide Nanomaterials: Synthesis, Properties, Modifications, and Applications", Chemical Reviews, 2007 Publication	<1 %
97	jestr.org Internet Source	<1 %
98	pure.iiasa.ac.at Internet Source	<1 %
99	Submitted to Higher Education Commission Pakistan Student Paper	<1 %

100	Submitted to Indian Institute of Technology, Kanpur Student Paper	<1%
101	Praachi Tiwari, Darshana Kapri, Amartya Pradhan, Angarika Balakrishnan, Pratik R Chaudhari, Vidita A Vaidya. "Chronic hM4Di-DREADD mediated chemogenetic inhibition of forebrain excitatory neurons in postnatal or juvenile life does not alter adult mood-related behavior", Cold Spring Harbor Laboratory, 2021 Publication	<1%
102	Submitted to University of Hong Kong Student Paper	<1%
103	docplayer.net Internet Source	<1%
104	eprints.soton.ac.uk Internet Source	<1%
105	Augusto Cesar Monteiro Silva. "Análise comparativa de abordagens para aprendizado de transformações imagem-a-imagem", Universidade de Sao Paulo, Agencia USP de Gestao da Informacao Academica (AGUIA), 2020 Publication	<1%

106	Mohan L. Verma, Homendra D. Sahu. "Ionic conductivity and dielectric behavior of PEO-based silver ion conducting nanocomposite polymer electrolytes", Ionics, 2015 Publication	<1 %
107	cronfa.swan.ac.uk Internet Source	<1 %
108	downloads.hindawi.com Internet Source	<1 %
109	scholar.lib.vt.edu Internet Source	<1 %
110	A. A. Sadeghi, T. Ebadzadeh, B. Raissi, S. Ghashghaie, S. M. A. Fateminia. " Application of the Multi-Step EPD Technique to Fabricate Thick TiO Layers: Effect of Organic Medium Viscosity on the Layer Microstructure ", The Journal of Physical Chemistry B, 2013 Publication	<1 %
111	Submitted to De Montfort University Student Paper	<1 %
112	Submitted to KTH - The Royal Institute of Technology Student Paper	<1 %
113	Rajan Jose. "Metal Oxides for Dye-Sensitized Solar Cells", Journal of the American Ceramic Society, 02/2009 Publication	<1 %

114	Shujahadeen B. Aziz. "Occurrence of electrical percolation threshold and observation of phase transition in chitosan(1−x):AgI x (0.05 ≤ x ≤ 0.2)-based ion-conducting solid polymer composites", Applied Physics A, 2016 Publication	<1 %
115	eee.iub.edu.bd Internet Source	<1 %
116	en.unionpedia.org Internet Source	<1 %
117	newweb.bose.res.in Internet Source	<1 %
118	pastel.archives-ouvertes.fr Internet Source	<1 %
119	Abrantes, J.C.. "Representations of impedance spectra of ceramics", Materials Research Bulletin, 20000401 Publication	<1 %
120	Ezgi Yılmaz Topuzlu, Burak Ulgut, Ömer Dag. " Role of Water in the Lyotropic Liquid Crystalline Lithium Iodide–Iodine–Water–C E Mesophase as a Gel Electrolyte in a Dye-Sensitized Solar Cell ", Langmuir, 2021 Publication	<1 %
121	Jung-Chuan Chou, Chang-Yi Wu, Yi-Hung Liao, Chih-Hsien Lai, Chung-Ming Yang, Pei-Hong	<1 %

You, Chien-Hung Kuo, Cheng-Chu Ko. "IGZO/TiO2 Composited Film as a Photoelectrode With Reduced Graphene Oxide/Pt Counter Electrode for a Dye-Sensitized Solar Cell", IEEE Journal of Photovoltaics, 2018
Publication

---

122 S.N. Karthick, K.V. Hemalatha, Suresh Kannan Balasingam, F. Manik Clinton, S. Akshaya, Hee - Je Kim. "Dye - Sensitized Solar Cells: History, Components, Configuration, and Working Principle", Wiley, 2019 <1%
Publication

---

123 Tamez Uddin, Yohann Nicolas, Céline Olivier, Thierry Toupance. "Low Temperature Preparation Routes of Nanoporous Semi-Conducting Films for Flexible Dye-Sensitized Solar Cells", American Chemical Society (ACS), 2013 <1%
Publication

---

124 Tripathi, S.K., Ramneek Kaur, and Mamta Rani. "Oxide Nanomaterials and their Applications as a Memristor", Solid State Phenomena, 2014. <1%
Publication

---

125 Zhang, Qifeng, and Guozhong Cao. "DYE-SENSITIZED SOLAR CELLS BASED ON NANO- <1%

STRUCTURED ZINC OXIDE", Annual Review of Nano Research, 2009.
Publication

126	citeseerx.ist.psu.edu Internet Source	<1 %
127	digital.library.ryerson.ca Internet Source	<1 %
128	etheses.dur.ac.uk Internet Source	<1 %
129	prr.hec.gov.pk Internet Source	<1 %
130	shodhganga.inflibnet.ac.in Internet Source	<1 %
131	www.jim.or.jp Internet Source	<1 %
132	Ahmed Mourtada Elseman, Mohamed M. Rashad, Ali M. Hassan. "Easily Attainable, Efficient Solar Cell with Mass Yield of Nanorod Single-Crystalline Organo-Metal Halide Perovskite Based on a Ball Milling Technique", ACS Sustainable Chemistry & Engineering, 2016 Publication	<1 %
133	Chin Wei Lai, Foo Wah Low, Siti Zubaidah Binti Mohamed Siddick, Joon Ching Juan. " Graphene/TiO Nanocomposites: Synthesis	<1 %

Routes, Characterization, and Solar Cell Applications ", Wiley, 2019
Publication

---

134 Da-Wei Liu, I-Chun Cheng, Jian Z. Chen, Hsin-Wei Chen, Kuo-Chuan Ho, Chin-Cheng Chiang. "Enhanced optical absorption of dye-sensitized solar cells with microcavity-embedded TiO_2 photoanodes", Optics Express, 2012 <1 %
Publication

---

135 DalSpace.library.dal.ca <1 %
Internet Source

---

136 Girija Nandan Arka, Shashi Bhushan Prasad, Subhash Singh. "Comprehensive study on dye sensitized solar cell in subsystem level to excel performance potential: A review", Solar Energy, 2021 <1 %
Publication

---

137 Gui Qiang Wang, Wei Xing, Shu Ping Zhuo. "A Novel Counter Electrode Based on Hierarchical Porous Carbon for Dye-Sensitized Solar Cells", Materials Science Forum, 2011 <1 %
Publication

---

138 Hsu, C.P.. "EIS analysis on low temperature fabrication of TiO"2 porous films for dye-sensitized solar cells", Electrochimica Acta, 20081030 <1 %
Publication

139	M. S. H. Choudhury, Shah Ridwan Ahmed, Md. Munirul Islam Tusher, Muhammad Athar Uddin, M. Shafiul Alam, T. Soga. "Optimization of Electrophoretic Deposition Parameters for Uniform Titanium Oxide Deposition on Conductive Glass Substrate", 2018 International Conference on Innovations in Science, Engineering and Technology (ICISET), 2018 Publication	<1 %
140	M.A. Brza, S.B. Aziz, H. Anuar, F. Ali. "Structural, ion transport parameter and electrochemical properties of plasticized polymer composite electrolyte based on PVA: A novel approach to fabricate high performance EDLC devices", Polymer Testing, 2020 Publication	<1 %
141	Tarek Azizi, Zouhour Kaddachi, Moufida Ben Karoui, Ala Eddinne Touihri, Rached Gharbi. " Electrical Characterization and Efficiency Enhancement of Dye Sensitized Solar Cell Using Natural Sensitizer and TiO Nanoparticles Deposited by Electrophoretic Technique ", IEEE Journal of Photovoltaics, 2021 Publication	<1 %
142	coek.info Internet Source	<1 %

143	digitalcommons.mcmaster.ca Internet Source	<1 %
144	solar.anu.edu.au Internet Source	<1 %
145	www.iiste.org Internet Source	<1 %
146	www.oak.go.kr Internet Source	<1 %
147	www.powershow.com Internet Source	<1 %
148	"Principles of Electroanalytical Methods", Environmental Applications of Instrumental Chemical Analysis, 2015. Publication	<1 %
149	A.P. Uthirakumar. "Chapter 19 Fabrication of ZnO Based Dye Sensitized Solar Cells", IntechOpen, 2011 Publication	<1 %
150	Om Parkash. "Preparation structure and dielectric behaviour of the system Sr1−xLaxTi1−xFexO3 (x ≤ 0.50)", Journal of Chemical Sciences, 10/2003 Publication	<1 %
151	Pouya Amrollahi, Jerzy S. Krasinski, Ranji Vaidyanathan, Lobat Tayebi, Daryoosh Vashaee. "Chapter 7-1 Electrophoretic	<1 %

Deposition (EPD): Fundamentals and Applications from Nano- to Micro-Scale Structures", Springer Science and Business Media LLC, 2015
Publication

152	Smart Sensors Measurement and Instrumentation, 2016. Publication	<1 %
153	Besra, L.. "A review on fundamentals and applications of electrophoretic deposition (EPD)", Progress in Materials Science, 200701 Publication	<1 %
154	Handbook of Nanoelectrochemistry, 2016. Publication	<1 %
155	Jihuai Wu, Zhang Lan, Jianming Lin, Miaoliang Huang, Yunfang Huang, Leqing Fan, Genggeng Luo. "Electrolytes in Dye-Sensitized Solar Cells", Chemical Reviews, 2015 Publication	<1 %
156	Moon, Jongyun, Aulis Tuominen, and Arho Suominen. "Forecasting a change in technology: are Dye-sensitised Solar Cells a source of ubiquitous energy?", International Journal of Technology Policy and Management, 2012. Publication	<1 %

157	N. Bonanos, B. C. H. Steele, E. P. Butler. "Applications of Impedance Spectroscopy", Wiley, 2005 Publication	<1 %
158	R. Vittal, Kuo-Chuan Ho. "Zinc oxide based dye-sensitized solar cells: A review", Renewable and Sustainable Energy Reviews, 2017 Publication	<1 %
159	Singh, Lakshmi K., Tado Karlo, and Arvind Pandey. "Electrochemical Impedance Spectroscopic Study on DSSC Sensitized with *Begonia malabarica* Lam.", Materials Science Forum, 2013. Publication	<1 %
160	eprints.utem.edu.my Internet Source	<1 %
161	dspace.lboro.ac.uk Internet Source	<1 %

Exclude quotes	On	Exclude matches	Off
Exclude bibliography	On		